University of Cincinnati

Date: 7/9/2021

I, Ryan P Caliguri, hereby submit this original work as part of the requirements for the degree of Master of Science in Mechanical Engineering.

It is entitled:

Comparison of Sensible Water Cooling, Ice building, and Phase Change Material in Thermal Energy Storage Tank Charging: Analytical Models and Experimental Data

Student's name: **Ryan P Caliguri**

This work and its defense approved by:

Committee chair: Michael Kazmierczak, Ph.D.

Committee member: Ahmed Elgafy,Ph.D.

Committee member: Sang Young Son, Ph.D.

40420

Comparison of Sensible Water Cooling, Ice building, and Phase Change Material in Thermal Energy Storage Tank Charging: Analytical Models and Experimental Data

A thesis submitted to the

Graduate School

of the University of Cincinnati

in partial fulfillment of the

requirements for the degree of

MASTER OF SCIENCE

In the Department of Mechanical and Materials Engineering

of the College of Engineering & Applied Sciences

by

Ryan Patrick Caliguri

Bachelor of Science in Engineering Physics, Xavier University, Cincinnati, Ohio, 2019

Committee Chair: Michael J. Kazmierczak, Ph.D., Associate Professor

Abstract:

In effort to both save operating expenses and be environmentally friendly, thermal energy storage provides a means for companies to handle daytime HVAC requirements while using off-peak (nighttime) electrical power. This paper sets out to compare three of the most common techniques used for thermal energy storage, by comparing both the analytical modeling of their energy storage and actual experimental data for their energy storage, using the same exact test apparatus for each of the techniques. The results of this experiment show that using normal HVAC temperatures, sensible water chilled to its maximum value after only about two hours, while PCM would take nearly six hours to achieve "linkage," or solidified material merging between the helix coils. Ice building, done with -7° coolant, took 4.5 hours to achieve linkage. Initial heat transfer was proportional to the difference between initial tank temperature and the coolant temperature, and went asymptotically towards zero for sensible as the temperature of the tank and coolant reach equilibrium. For ice, the heat transfer rate was always more than twice that of PCM during latent storage, which is attributed to the difference between coolant temperatures and freezing points for the respective materials. Sensible water cooldown would require 232.8% of the tank volume to store the same energy relative to the environment compared to ice building, and 126.3% of the tank volume compared to phase change material. This is to be weighed with the benefit of using existing HVAC condensing units to chill the water, and the fact that water itself is inexpensive. The high latent heat of freezing for water meant it held more energy than both the water sensible cooldown and PCM freezing, but with the downside of requiring medium temperature condenser units in order to be efficient (instead of the high temperature units used in typical HVAC). After 4.5 hours, PCM would surpass the energy stored in the same volume as water sensibly, due to its latent energy storage, while also utilizing ordinary HVAC temperatures, but is relatively costly as a medium, especially when compared to water.

Table of Contents

Acknowledgements

I would like to thank my advisor, Dr. Michael Kazmierczak, for not only teaching me the fundamentals of thermal energy storage in his class, but also for supporting me with his wealth of knowledge on the subject matter throughout my research. Thanks to his help, it was possible to complete this thesis with both analytical and experimental components while also completing coursework and acting as a teaching assistant and lab instructor.

I would also like to thank Dr. Sang Young Son and Dr. Ahmed Elgafy for serving on my thesis committee, without them this also would not be possible.

List of Figures

List of Tables

Nomenclature

Variable	
ENGLISH	
A_{pipe}	Convection Area of the Pipe
$C_{coolant}$	Heat Capacity of the Coolant
$C_{tank(water)}$	Heat Capacity of the Storage Media
$D_{inner\ tube}$	Inner Diameter of Tube
$D_{outer\ tube}$	Outer Diameter of Tube
$dT_{coolant}$	Temperature Change of Coolant
h_{inner}	Heat Transfer Coefficient on Inner Tube Wall
k	Frozen Storage Material Thermal Conductivity
k_{ice} , k_{PCM}	Thermal Conductivity of Ice or PCM
k_{tube}	Thermal Conductivity of Tube Wall Material
L_{ice} , L_{PCM}	Latent Heat Capacity of Ice or PCM
L_{tube}	Length of Tube in Coil
$\dot{m}$	Mass Flow Rate of Coolant
r	Instantaneous Ice or Frozen PCM Radius
r_o	Outer Radius of Pipe
s	Ice or Frozen PCM Radius
t	Time
T_∞	Ambient Temperature
$T_{coolant(in)}$	Temperature of Coolant upon Entering Storage System
$T_{coolant(out)}$	Temperature of Coolant upon Exiting Storage System
$T_{coolant}$	Coolant Temperature
$T_{freezing}$	Freezing Temperature of Storage Media
T_{tank}	Instantaneous Tank Temperature
U	Overall Heat Transfer of Pipe for Freezing Processes
UA_{bucket}	Overall Heat Transfer Coefficient of the Outer Bucket Wall
U_{pipe}	Overall Heat Transfer Coefficient of Pipe for Sensible
V_{tank}	Volume of Tank
GREEK	
ρ_{ice} , ρ_{PCM}	Density of Ice or PCM
ρ	Density of Storage Media

Introduction and Objective

The process of thermal energy storage is not a new concept, even though its forms have changed substantially over time. Thousands of years ago, cultures who lived in deserts often built homes with very thick walls which created a thermal mass, effectively allowing them to "store" the cold of the night for hot days, and the warmth of the days for cold nights. More recently, in the past hundreds of years, people in seasonal climates would go to bodies of water in the winter and saw blocks of ice out of them, which were stored in "ice houses," packed in thick layers of saw dust as a form of insulation. Stored this way, the ice would last often into the summer, and allow for chilling of food and beverages (Cummings, 1989).

With the advent of modern freon-based HVAC and chilling systems, it seemed as though the need for such storage was all but gone. But somewhat ironically, when such systems once reserved for medical facilities and movie theaters were made common for every home and business, other issues arose. Namely was the fact that the demand for such cooling techniques was not consistent, but periodic with the time of day; in the middle of the night there is very little cooling demand and in the afternoon on hot days there is a massive demand, and electricity demand is directly proportional. Electricity production, especially for methods viewed as "green" or "greener" such as wind nuclear, are not so readily modulated to fit demand, but are rather slow response or dependent on nature. When consumers all turn on their air conditioning on a hot day, the spike is often met with quick-response oil and natural gas-fired units. This use of fossil fuels not only poses environmental issues, but also makes this energy far more costly. These costs are reflected in "time-of-day" rates and demand charges common for commercial energy clients and becoming more popular with residential clients, where energy is substantially cheaper at night (Lindsay and Andrepont, 2019).

These “time-of-day” energy rates and demand charges are the primary reason for the resurgence of thermal energy storage. By running a refrigeration unit at night to chill a sufficient volume of a thermal energy storage (TES) media to handle the HVAC energy requirements of the day, facilities are able to take advantage of substantially lower electricity costs. Facilities shifting their energy usage to what would normally be a trough in the overall power demand curve also means that the generation requirements are “smoothed,” or rather are consistent over the course of the day, and not dependent on fast-response fossil fuel units to meet a peak in demand. This technique, therefore, offers a rare intersection of cost-saving and “green.”

If a facility decides to invest in a TES system, they will subsequently find that there are numerous options for storage media, each with their own benefits and drawbacks. One option is sensible water storage, where water is chilled down to slightly above its freezing point, but not frozen. Another option is to actually freeze the water in a TES process known as “ice-building.” Yet a third option comes in the form of phase change material (PCM), which, as its name implies, freezes at a different temperature than water. Each of these methods have been studied extensively on their own, so what this thesis shall serve to do is offer an in-depth analytical model for the storage process in each type of system, paired with experimental data to match, where all three media are chilled in the same vessel. This shall allow those interested in TES to have a fair comparison of the three techniques, as well as the tools necessary to model a proposed system.

Literature Review

For the sake of this thesis, a variety of sources were required to combine theory and practice in a way that was grounded in reality, and applicable to the current field of HVAC. These sources include those used to provide historical context of thermal energy storage as a field, those which describe current thermal energy storage systems in use and how they are sized, those which describe Stefan-Type freezing problems, those which describe the specific coiled ice-on-tube internal melt configuration utilized in the experimental test vessel, and those which describe various parameters and phenomena occurring in thermal energy storage.

One of the most comprehensive papers referenced, touching on nearly all of the above subjects, is Cumming's paper titled "Modeling, Design, and Control of Partial Ice-Storage Air-Conditioning Systems." This paper begins discussing the history of thermal energy storage with ice harvesting, continues to discuss energy demand and production as context for the need of thermal energy storage today, then discusses a number of systems currently in use. Furthermore, it goes on to summarize the condensing units used, the equations applicable to thermal energy storage and discharge, and even simulates such processes (Cummings, 1989).

Another paper critical to understanding the development of thermal energy storage systems from the time of sawing ice blocks out of rivers and lakes to present is Lindsay's article in ASHRAE titled "Evolution of Thermal Energy Storage for Cooling Applications." This article not only explains various techniques and medias utilized, but also offers samples of facilities where each has been implemented (Lindsay and Andrepont, 2019).

With a grasp on what the thermal energy storage industry had developed from, it is then important to understand previous work to connect theory to practice. One such previous work is Jekel's "Modeling of Ice-Storage Tanks." Here, cylindrical tube geometry is analyzed for ice building with brine

solution as a working fluid, using energy balances and various dimensionless parameters to arrive at empirical relations to describe heat transfer of the system, and the effectiveness of a tank design (Jekel et al., 1993).

While empirical relations are limited in their scope of applicability, it is apparent from them as well as in data from systems, that as ice grows on a tube, it acts to insulate it the tank fluid from the coil (apparent in the heat transfer rate declining with growth). Various methods are used to mitigate this effect, one of which is described in Kazmierczak's "Heat transfer augmentation for external ice-on-tube TES systems using porous copper mesh to increase volumetric ice production." This paper describes how a porous copper mesh may serve as a sort of extended surface for a coil, allowing it to conduct through ice and convect into the freezing fluid with less resistance. While such a method was only tested in a water tunnel (where the freezing fluid had a velocity), many of the same principles apply to a tank of motionless fluid. For future studies on the tank system used in this thesis, such an enhancement technique could be applied (Kazmierczak and Nirmalanandhan, 2006).

Similar to the previous paper, Intemann's "Heat transfer and ice formations deposited upon cold tube bundles immersed in flowing water—I, Convection Analysis" deals with a flowing storage media, but this paper deals with the effect of changing whole tube array arrangements, as well as flow parameters. While the experimental setup for this thesis did not involve a flowing storage media, if a future study were to have the freezing coils in a flow of storage media, this paper would aid in the optimization of such a system (Intemann and Kazmierczak, 1997).

One source directly applicable to this thesis was Manlapaz's "Fully Developed Laminar Convection From a helical Coil." In this work, a relation is found for a helically coiled tube's Nusselt number by compiling data from numerous experiments. This compilation allows Manlapaz to develop a relation good for all Dean numbers and all Prandtl numbers. Due to the differing flow rates and coolant

properties throughout this thesis, such a broadly applicable Nusselt relation is indispensable (Manlapaz and Churchill, 1981).

Another critical resource for developing a cylindrical Stefan solution was Bejan's "Heat Transfer Handbook." Along with planar and spherical geometries, this handbook goes into a simpler form of the quasi-steady Stefan solution for cylindrical outward freezing. Although this formulation neglects the wall conduction resistance of the tube, it provided a basic equation to check the final derivation against (Bejan and Kraus, 2003).

After the analytical theory was sorted out, pre-trials of the experiment began. One phenomenon seen during these pre-trials in the thermocouple data was the supercooling of liquid water below its nominal freezing point at atmospheric pressure. Although thought to be erroneous at first, upon researching articles such as Chen's "A study of supercooling phenomenon and freezing probability of water inside horizontal cylinders," it was discovered that supercooling of water occurs often, when there is an absence of a nucleation source. This supercooling of water occurred in every latent ice trial, but not in the PCM latent runs (Chen and Lee, 1998).

Another phenomenon experienced in all early water pre-trials was the stratification of the tank. Wildin's "Stratified Thermal Storage. A new/old Technology" focuses on this phenomenon, explaining that this is the separation of the tank water into a warmer top region and colder bottom region, by virtue of the density dependence of water on temperature; in general, warm water is less dense than cooler water (with an exception near the freezing point of water where the density decreases once again). Wildin's paper continues on to explain how stratification is used currently for thermal energy storage, with multiple samples of current facilities using it. The paper makes note of how the stratification is a fragile state within a tank, and it was this insight that led to the inclusion of a bubbler

for the water trials in this thesis. The bubbling action inhibits such stratification, allowing the tank temperature to uniformly change (in this case, decrease) (Wildin et al., 1990).

Once the experimental data was collected for this thesis, it was then necessary to process the data. As with any experimental data there is some level of uncertainty, and in order to properly analyze this uncertainty, Coleman's "Experimentation and Uncertainty Analysis for Engineers" served as a guide. With this, the level of uncertainty coming from thermocouples, scales, flow meters, and calipers were formulated and their error traced through equations (Coleman and Steel, 1989).

For the sake of this thesis, the quasi-steady approximation was valid for the analytical model due to the low Stefan number for both ice and PCM runs. While this would be the case for many latent thermal energy storage systems, there are systems where the sensible component of the cooldown may not be substantially lower than the latent storage (equating to a higher Stefan number, see Appendix A). For such a case, numerical methods could be employed, or a method similar to that used by Khalid in "*An analytical method for the solution of two phase Stefan problem in cylindrical geometry."* This paper sets forth a method to find an analytical solution for cylindrical Stefan problems with higher Stefan numbers through a separation of variables technique, utilizing computer software to find Eigenvalues. (Khalid et al., 2019).

Another approximate solution to the cylindrical Stefan problem is set forth in Caldwell's "Numerical solution of one-phase Stefan problems by the heat balance integral method, Part I—cylindrical and spherical geometries." The method utilized here is the Heat Balance Integral Method, previously described by Goodman, and originating in Prandtl-Von Karman's "Boundary Layer Method." Much of this paper is dedicated to tuning this "Heat Balance Integral method" to compensate for its substantial oversimplifications, such as assuming there is a single temperature profile over the whole domain of the system (Caldwell and Chiu, 2000).

For this thesis, Puretemp-8 was chosen as the phase change material due to two main criteria; one was that it could be frozen with temperatures achieved in a common HVAC system, and the other was that it would still have a large enough temperature differential with the air it would condition (by means of some intermediate fluid) that it would still be effective. This phase change material is only one of many though. Pereira da Cunha reviews a vast array of phase change materials in "Thermal energy storage for low and medium temperature applications using phase change materials – A review," and these materials range from organic substances like paraffin waxes, to inorganic salts, and even substances that undergo thermochemical reactions. These materials are not limited to cooling applications such that described in this thesis, either, but may also be utilized for heating as Pereira da Cunha describes (Pereira da Cunha and Eames, 2016).

Experimental Setup

As mentioned in the introduction, the same apparatus was utilized for testing all three storage techniques. This apparatus (shown in Figures 1 and 2) included a freon-to-liquid chiller (NESLAB RTE-140) whose chilled liquid passed through an Omega FPR300 Low Flow Meter (Item 10), to a helical coil contained in the test vessel (item 15) made of polyethylene and length 5.58 m with Inner diameter of 12.7 mm and outer diameter of 15.88 mm. Shown in Figure 2, this helical coil is submerged in a 5-gallon bucket made of high-density polyethylene that is insulated on top, sides, and bottom by 19.05mm thick K-flex brand flexible sheet insulation. The bottom of the bucket also sits on a 38.1 mm thick sheet of Owens Corning rigid foam insulation and is therefore considered adiabatic in the analytical model. The temperature is probed using Omega high accuracy T-type thermocouples on the cold water exit (Item 8) from the chiller, three depths within the center of the bucket on a fiberglass rake (items 1-3), at three positions on the surface of the helical coil (items 4-6), at the return line to the chiller (item 7), and in the lab room to get ambient temperature [at a position protected from any convection from the condensing coil fan of the water chiller (item 9)].

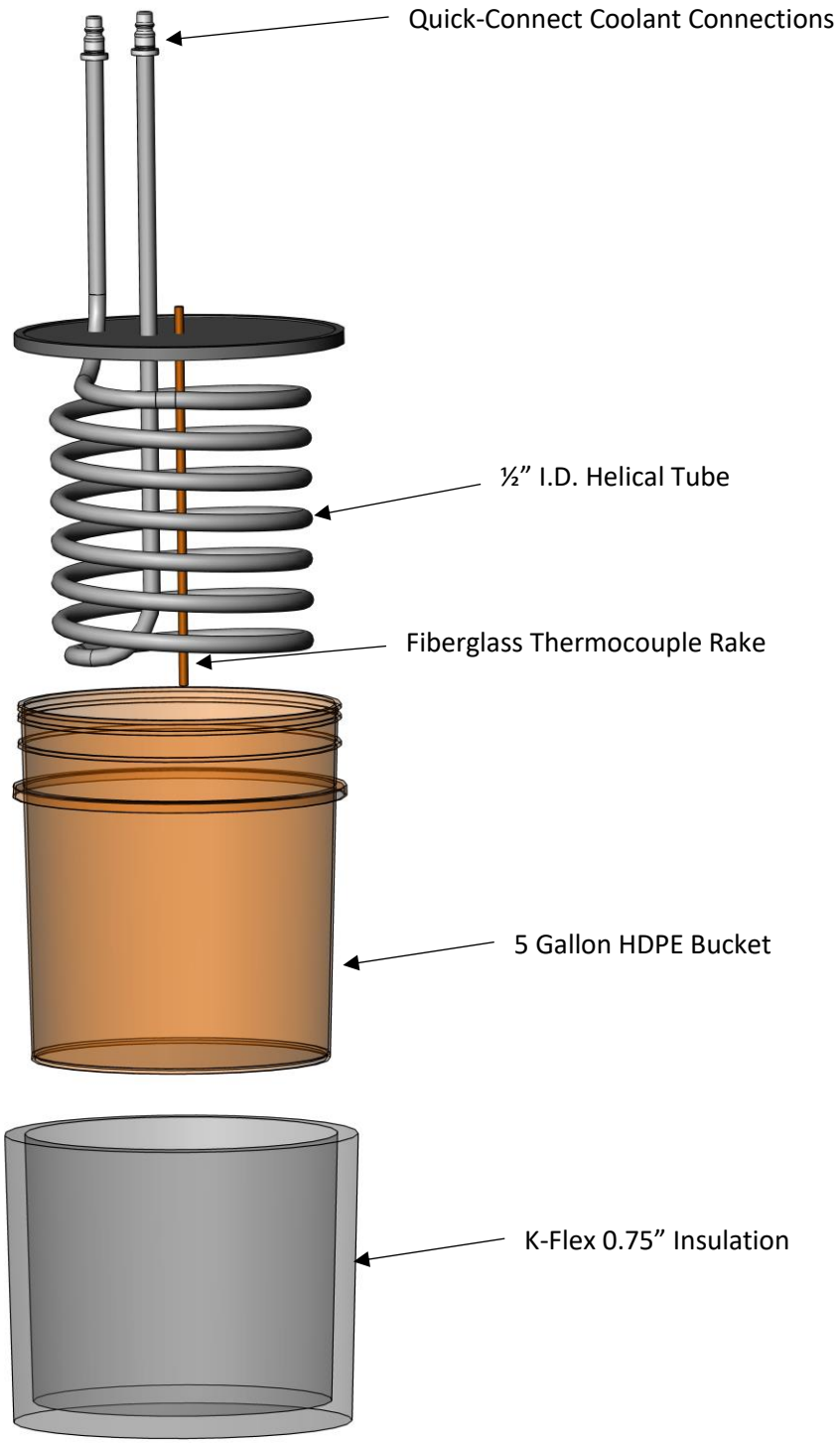

Figure 1. Test Vessel Exploded View

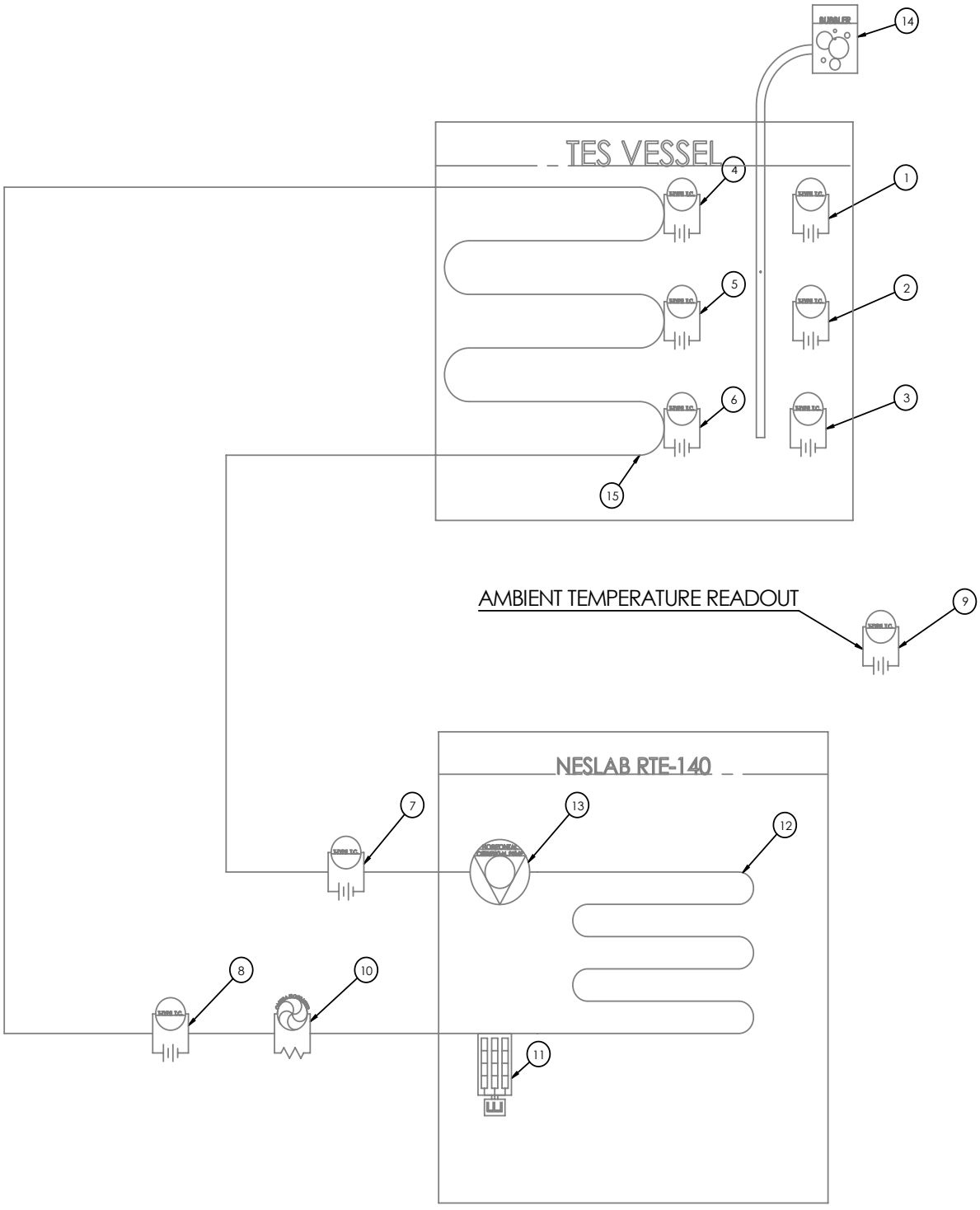

Figure 2. P&ID For Test System

Table 1. P&ID Components

ITEM NUMBER	PART
1	UPPER TANK THERMOCOUPLE (ON CENTER RAKE)
2	MID TANK THERMOCOUPLE (ON CENTER RAKE)
3	LOWER TANK THERMOCOUPLE (ON CENTER RAKE)
4	INLET COIL SURFACE THERMOCOUPLE (ON SURFACE OF COOLING COIL)
5	MID COIL SURFACE THERMOCOUPLE (ON SURFACE OF COOLING COIL)
6	EXIT COIL SURFACE THERMOCOUPLE (ON SURFACE OF COOLING COIL)
7	COOLING FLUID SEND THERMOCOUPLE
8	COOLING FLUID RETURN THERMOCOUPLE
9	AMBIENT TEMPERATURE THERMOCOUPLE
10	OMEGA LOW-FLOW METER
11	HEATING ELEMENT
12	HEAT EXCHANGER WITH CHILLER EVAPORATOR COIL
13	PUMP
14	ELECTRIC BUBBLER
15	PLASIC COIL FOR STORAGE VESSEL

Experimental Procedure and Runs

In pre-trials, it was found that the tank stratified, or separated by density of water, which is a function of temperature. This was mitigated in all formal runs with the addition of a small electric bubbler to agitate the liquid in the tank. For both the sensible water cool down and PCM freezing, the cooling liquid was pure water held at a set point of 4.0°C, typical for the evaporator coil temp of a regular HVAC system. For the ice freezing trial, the cooling liquid was 30% ethylene glycol 70% water by mass, held at -7C. After pre-trials, three final experiments were run, one for each of the three conditions. Table 2 below describes the conditions for each.

The sensible experiment was ran from ambient temperature to steady state equilibrium, while the ice and PCM runs were conducted from a tank of media at ambient temp until the respective media froze to linkage. For the two latent energy storage cases, there was initially a sensible cooldown to near the media freezing point, followed by a build of frozen material on the coil. Measurements of frozen ice and PCM material were conducted at 20 minute intervals (with an exception of two 40 minute intervals for PCM at large time to avoid excessive agitation) using calipers as well as a hanging scale, from which the coil/lid assembly was hung. Coolant flow rate was held throughout each run, but varied some between experiments due to the coolant properties, as well as plumbing geometry changes that were inevitable using flexible tube. Temperature data was recorded for various locations (see Figure 2) every 0.610 seconds using a data acquisition unit, and depending on the full experiment duration, the data collected was compressed by DaqPro software.

Table 2. Final Run Parameters

Parameter	Sensible Water Experiment	Ice Building Experiment	PCM Freezing Experiment
Initial Tank Temperature (°C)	19.1	16	22
Coolant Composition	100% Water	70% Water 30% Ethelene Glycol (By mass)	100% Water
Coolant Flow Rate (GPM)	2.19	0.91	1.5
Coolant Density (kg/m^3)	999.4	1,063	999.4
Coolant Dynamic Viscosity ($N.s/m^2$)	1.21E-03	4.89E-03	1.21E-03
Coolant Thermal Conductivity ($W/m^2°C$))	0.585	0.466	0.585
Length of Coil (m)	5.58	5.58	5.58
Ambient Temperature (°C)	16.9	15.1	22
Coolant Inlet Temperature (°C)	4.5	-6.1	4.5
Reynolds Number	11,441	1,251.20	7,836
Prandtl Number	8.664	37.45	8.6644
Nusselt Number	53.08	18.1959	43.9733
Dean Number	2,620	286.57	1795
Stefan Number	NA	0.0268	0.0315

Analytical Modelling

In order to compare the three tank cool-downs and storage capacities, analytical models shall be derived here to describe each, starting with the fundamental equations of heat transfer.

Sensible Cooldown:

To describe the cooldown of the sensible tank, the energy balance of the coolant tube must first be derived. This is done as follows by equating the First Law of Thermodynamics to Newton's Law of Cooling, modified with wall resistance, via overall U-value [see Figure 3 (top)].

$$\dot{m}C_{coolant}dT_{coolant} = U_{pipe}[T_{tank} - T_{coolant}]A_{pipe} \tag{1}$$

By solving the above differential equation, the temperature of the coolant exiting the heat exchanger of the tank may be predicted as a function of the tank temperature of the coolant entering the heat exchanger and the temperature of the tank itself.

$$T_{coolant(out)} = T_{tank} + \left[T_{coolant(in)} - T_{tank}\right]e^{\frac{-(UA)_{pipe}}{\dot{m}C_{coolant}}} \tag{2}$$

This result is then used as follows in the energy balance of the tank media so that the only unknown value is the tank temperature as a function of time. Here, the First Law of the tank is equated to the First Law for the coolant plus Newton's Law of Cooling applied to the tank itself, taking into account the heat gain of the tank from the vessel's surroundings [See Figure 3 (bottom)].

$$\rho V_{tank}C_{tank(water)}\frac{dT_{tank}}{dt} = \dot{m}C_{coolant}\left[T_{coolant(in)} - T_{coolant(out)}\right] + UA_{bucket}[T_{\infty} - T_{tank}] \tag{3}$$

$$\rho V_{tank}C_{tank(water)}\frac{dT_{tank}}{dt} = \dot{m}C_{coolant}\left[T_{coolant(in)} - \left[T_{tank} + \left[T_{coolant(in)} - T_{tank}\right]e^{\frac{-(UA)_{pipe}}{\dot{m}C_{coolant}}}\right]\right] + UA_{bucket}[T_{\infty} - T_{tank}]$$

$$\frac{dT_{tank}}{dt} + T_{tank}\left[\frac{\dot{m}C_{coolant} - \dot{m}C_{coolant}e^{\frac{-(UA)_{pipe}}{\dot{m}C_{coolant}}} + UA_{bucket}}{\rho V_{tank}C_{tank(water)}}\right] = \left[\frac{T_{coolant(in)}\left(\dot{m}C_{coolant} - \dot{m}C_{coolant}e^{\frac{-(UA)_{pipe}}{\dot{m}C_{coolant}}}\right) + UA_{bucket}T_{\infty}}{\rho V_{tank}C_{tank(water)}}\right] \quad (4)$$

This result may be recognized as a first order non-homogeneous ordinary differential equation (ODE), whose constants will be simplified as follows.

$$\frac{dT_{tank}}{dt} + aT_{tank} = b \quad (5)$$

For the homogenous solution, the constant b is set to zero.

$$\frac{dT_{tank}}{dt} + aT_{tank} = 0 \quad (6)$$

The following characteristic equation is then used.

$$s + a = 0 \quad (7)$$

$$s = -a$$

$$T_{tank}(t) = Ae^{st} = Ae^{-at} \quad (8)$$

Then returning to the particular solution:

$$\frac{dT_{tank}}{dt} + aT_{tank} = b$$

Since the forcing function is a constant, the particular solution is as well.

$$T_{tank(p)} = B \quad (9)$$

This constant value is then inserted back into the ODE.

$$0 + aT_{tank(p)} = b$$

$$T_{tank(p)} = \frac{b}{a} \tag{10}$$

$$T_{tank}(t) = T_{tank(p)} + T_{tank(homo)}(t) \tag{11}$$

$$T_{tank}(t) = Ae^{-at} + \frac{b}{a} \tag{12}$$

With initial condition that the starting temperature of the tank is some initial temperature.

$$t = 0, \qquad T_{tank}(0) = T_{initial} \tag{13}$$

$$T_{initial} = A + \frac{b}{a}$$

$$A = T_{initial} - \frac{b}{a}$$

$$T_{tank}(t) = \left(T_{initial} - \frac{b}{a}\right)e^{-at} + \frac{b}{a} \tag{14}$$

Where

$$\frac{b}{a} = \left[\frac{T_{coolant(in)}\left(\dot{m}C_{coolant} - \dot{m}C_{coolant}e^{\frac{-(UA)_{pipe}}{\dot{m}C_{coolant}}}\right) + UA_{bucket}T_{\infty}}{\rho V_{tank}C_{tank(water)}}\right]\left[\frac{\rho V_{tank}C_{tank(water)}}{\dot{m}C_{coolant} - \dot{m}C_{coolant}e^{\frac{-(UA)_{pipe}}{\dot{m}C_{coolant}}} + UA_{bucket}}\right]$$

$$\frac{b}{a} = \left[\frac{T_{coolant(in)}\left(\dot{m}C_{coolant} - \dot{m}C_{coolant}e^{\frac{-(UA)_{pipe}}{\dot{m}C_{coolant}}}\right) + UA_{bucket}T_{\infty}}{\dot{m}C_{coolant} - \dot{m}C_{coolant}e^{\frac{-(UA)_{pipe}}{\dot{m}C_{coolant}}} + UA_{bucket}}\right] \tag{15}$$

Finally, by combining all of this into the ODE, the final equation for the sensible cool down is derived, with tank temperature as a function of time.

$$T_{tank}(t) = \left(T_{initial} - \left[\frac{T_{coolant(in)}\left(\dot{m}C_{coolant} - \dot{m}C_{coolant}e^{\frac{-(UA)_{pipe}}{\dot{m}C_{coolant}}}\right) + UA_{bucket}T_{\infty}}{\dot{m}C_{coolant} - \dot{m}C_{coolant}e^{\frac{-(UA)_{pipe}}{\dot{m}C_{coolant}}} + UA_{bucket}}\right]\right)e^{-\left(\frac{\dot{m}C_{coolant} - \dot{m}C_{coolant}e^{\frac{-(UA)_{pipe}}{\dot{m}C_{coolant}}} + UA_{bucket}}{\rho V_{tank}C_{tank(water)}}\right)t} + \left[\frac{T_{coolant(in)}\left(\dot{m}C_{coolant} - \dot{m}C_{coolant}e^{\frac{-(UA)_{pipe}}{\dot{m}C_{coolant}}}\right) + UA_{bucket}T_{\infty}}{\dot{m}C_{coolant} - \dot{m}C_{coolant}e^{\frac{-(UA)_{pipe}}{\dot{m}C_{coolant}}} + UA_{bucket}}\right] \tag{16}$$

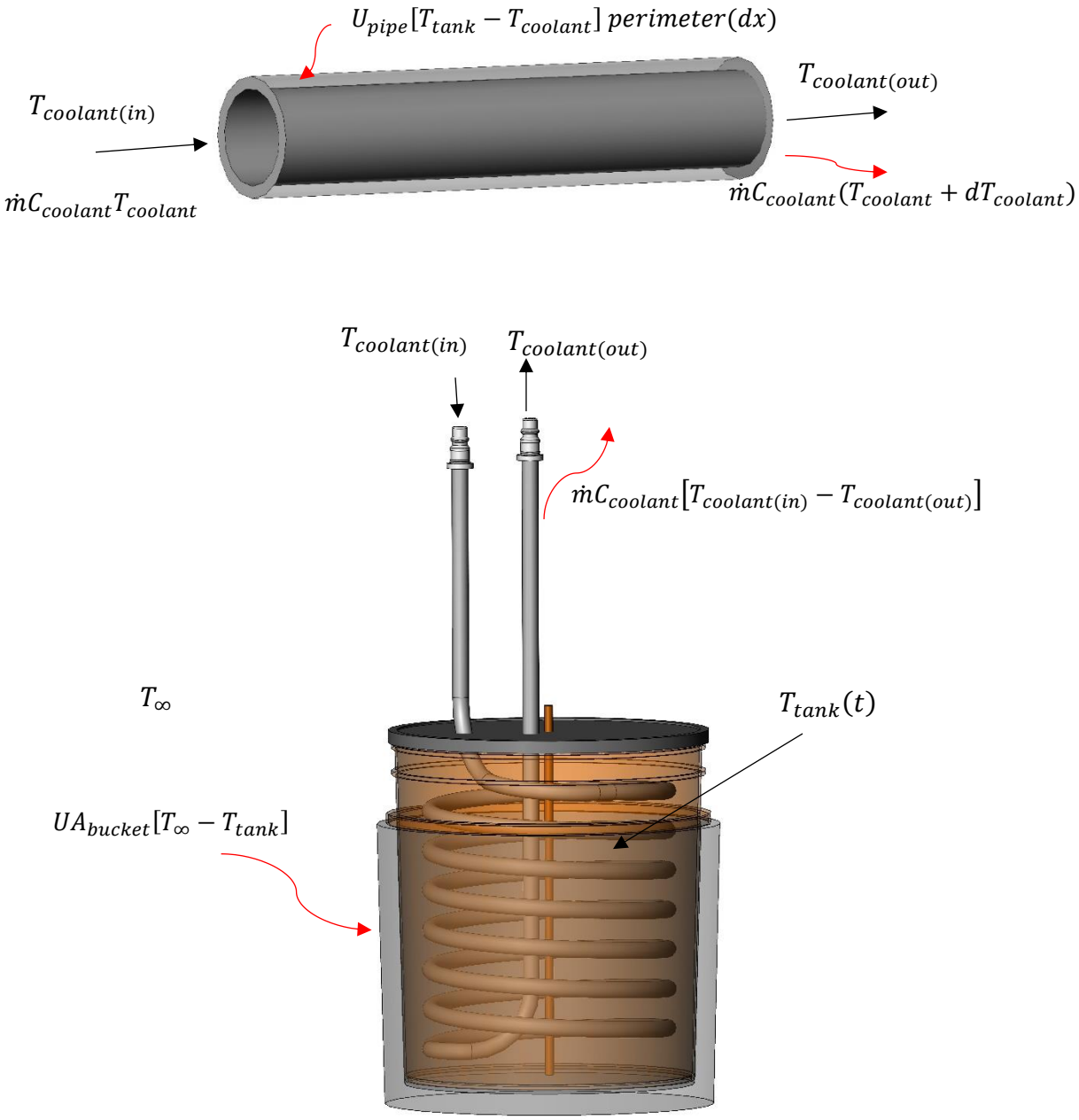

Figure 3. Temperatures and Energy Balances Used in Sensible Model

Latent (Ice/PCM Building)

For *planar* geometries, an exact solution exists for the Stefan problem of ice building (Yener and Kakaç, 2008). In this geometry it is seen that for very low Stefan Number, the difference between the exact solution and the quasi-steady solution (where heat in is equal to heat out, or the derivative of temperature with respect to time is almost zero) is negligible. For *cylindrical* geometry, however, an exact solution does not exist, but the quasi steady solution does exist (derived in detail below) and is once again appropriate for low Stefan Number conditions (Bejan and Kraus, 2003). Calculation of the Stefan Number is shown in Appendix A.

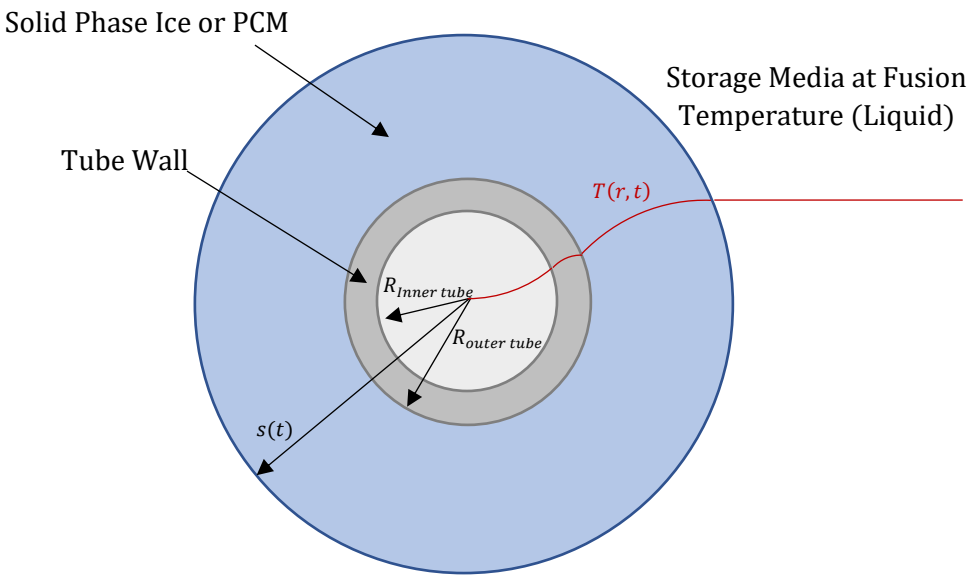

Figure 4. Cross Section of the Coil during Ice and PCM Building

For cylindrical ice building, the one-dimensional heat conduction equation with the quasi-steady assumption is as follows, where r_o is the outer wall radius of the tube, r is the radius of ice, and s(t) is the radius of the ice/liquid boundary as a function of time.

$$\frac{1}{r}\frac{\partial}{\partial r}r\frac{\partial T}{\partial r} = 0 \ (quasi\ steady\ approximation) \tag{17}$$

$$r_o < r < s(t)$$

The first boundary condition set Fourier's Law equal to Newton's Law of cooling at the ice to tube interface, where the conduction through the ice is equal to the convection and conduction from the coolant through the tube wall (U accounts for the combined series resistance of the inner convection of the tube as well as the conduction through the tube wall).

$$k_{ice}\frac{\partial T}{\partial r}\Big|_{r\,=\,r_o} = U[T(r_o,t) - T_{coolant}] \tag{18}$$

The second boundary condition states that the temperature at the ice-liquid interface is the freezing temperature of the liquid.

$$T(r,t)|_{r\,=\,s(t)} = T_{freezing} \tag{19}$$

The initial condition states that the initial ice radius is the outer radius of the tube.

$$s(0) = r_o \tag{20}$$

The overall heat transfer coefficient for the tube is as follows, where there is convection on the inner wall from the coolant, and conduction through the annular tube wall. It is set in terms of the outer surface area of the tube for the following calculations, as this is where the ice meets the tube.

$$U = \left[\frac{\pi D_{outer\ tube} L_{tube}}{\pi D_{inner\ tube} L_{tube} h_{inner}} + \frac{\pi D_{outer\ tube} L_{tube} * \ln\left(\frac{R_{outer\ tube}}{R_{Inner\ tube}}\right)}{2\pi k_{tube} L_{tube}} \right]^{-1}$$

$$U = \left[\frac{D_{outer\ tube}}{D_{inner\ tube} h_{inner}} + \frac{D_{outer\ tube} * \ln\left(\frac{R_{outer\ tube}}{R_{Inner\ tube}}\right)}{2k_{tube}} \right]^{-1} \quad (21)$$

Integrating the general equation, the temperature as a function of radius and time is as follows.

$$T(r,t) = C_1 \ln(r) + C_2 \quad (22)$$

Applying boundary Conditions:

$$k_{ice} \left. \frac{\partial [C_1 \ln(r) + C_2]}{\partial r} \right|_{r = r_o} = U\,[C_1 \ln(r_o) + C_2 - T_{coolant}]$$

$$k_{ice} \frac{C_1}{r_o} = U\,[C_1 \ln(r_o) + C_2 - T_{coolant}] \quad (23)$$

And:

$$T(r,0) = T_{freezing} = C_1 \ln(s) + C_2$$

$$C_2 = T_{freezing} - C_1 \ln(s) \quad (24)$$

Therefore

$$k_{ice} \frac{C_1}{r_o} = U\left[C_1 \ln(r_o) + \left(T_{freezing} - C_1 \ln(s)\right) - T_{coolant}\right]$$

$$k_{ice} \frac{C_1}{r_o} = U\left(C_1 \ln\left(\frac{r_o}{s}\right)\right) + U\left(T_{freezing} - T_{coolant}\right)$$

$$\frac{k_{ice}}{r_o} - U\left(\ln\left(\frac{r_o}{s}\right)\right) = \frac{U\left(T_{freezing} - T_{coolant}\right)}{C_1}$$

$$C_1 = \frac{T_{freezing} - T_{coolant}}{\frac{k_{ice}}{r_o U} + \ln\left(\frac{s}{r_o}\right)} \quad (25)$$

And thus:

$$T(r,t) = \left(\frac{T_{freezing} - T_{coolant}}{\frac{k_{ice}}{r_o U} + \ln\left(\frac{s}{r_o}\right)}\right)\ln(r) + T_{freezing}\left(\frac{T_{freezing} - T_{coolant}}{\frac{k_{ice}}{r_o U} + \ln\left(\frac{s}{r_o}\right)}\right)\ln(s)$$

$$T(r,t) = \left(\frac{T_{freezing} - T_{coolant}}{\frac{k_{ice}}{r_o U} + \ln\left(\frac{s}{r_o}\right)}\right)\ln\left(\frac{r}{s}\right) + T_{freezing} \tag{26}$$

Then, the Stefan Condition is applied, which equates the energy removed through the ice by conduction to the growth of the ice as a function of its latent heat of freezing, in radial geometry for this case.

$$k_{ice}\frac{\partial T}{\partial r}\Big|_{s(t)} = \rho_{ice} L_{ice}\frac{ds}{dt} \tag{27}$$

$$k_{ice}\frac{\partial}{\partial r}\left[\left(\frac{T_{freezing} - T_{coolant}}{\frac{k_{ice}}{r_o U} + \ln\left(\frac{s(t)}{r_o}\right)}\right)\ln\left(\frac{r}{s}\right) + T_{freezing}\right]\Bigg|_{r\,=\,s(t)} = \rho_{ice} L_{ice}\frac{ds}{dt}$$

$$k_{ice}\left(\frac{T_{freezing} - T_{coolant}}{\frac{k_{ice}}{r_o U} + \ln\left(\frac{s(t)}{r_o}\right)}\right)\frac{\partial}{\partial r}\left[\ln\left(\frac{r}{s}\right) + T_{freezing}\right]\Bigg|_{r\,=\,s(t)} = \rho_{ice} L_{ice}\frac{ds}{dt}$$

$$k_{ice}\left(\frac{T_{freezing} - T_{coolant}}{\frac{k_{ice}}{r_o U} + \ln\left(\frac{s(t)}{r_o}\right)}\right)\frac{1}{s(t)} = \rho_{ice} L_{ice}\frac{ds}{dt}$$

$$\frac{k_{ice}\left(T_{freezing} - T_{coolant}\right)}{\rho_{ice} L_{ice}} = \left(\frac{k_{ice}}{r_o U} + \ln\left(\frac{s(t)}{r_o}\right)\right)s(t)\frac{ds}{dt}$$

$$\int \frac{k_{ice}\left(T_{freezing} - T_{coolant}\right)}{\rho_{ice} L_{ice}}dt = \int \left(\frac{k_{ice}}{r_o U} + \ln\left(\frac{s(t)}{r_o}\right)\right)s(t)ds$$

$$\frac{k_{ice}\left(T_{freezing} - T_{coolant}\right)}{\rho_{ice} L_{ice}}t = \frac{1}{2}s^2\ln\left(\frac{s(t)}{r_o}\right) + \frac{1}{4}\left(\frac{2k_{ice}}{r_o U} - 1\right)s^2 + C$$

$$t = \left(\frac{\rho_{ice} L_{ice}}{k_{ice}\left(T_{freezing} - T_{coolant}\right)}\right)\left[\frac{1}{2}s^2\ln\left(\frac{s(t)}{r_o}\right) + \frac{1}{4}\left(\frac{2k_{ice}}{r_o U} - 1\right)s^2 + C\right] \tag{28}$$

With the previously mentioned initial condition,

$$s(0) = r_o$$

$$0 = \left(\frac{\rho_{ice} L_{ice}}{k_{ice}\left(T_{freezing} - T_{coolant}\right)}\right)\left[\frac{1}{2}{r_o}^2\ln\left(\frac{r_o}{r_o}\right) + \frac{1}{4}\left(\frac{2k_{ice}}{r_o U} - 1\right){r_o}^2 + C\right]$$

Combining constants:

$$0 = \left(\frac{k_{ice}}{2r_oU} - \frac{1}{4}\right){r_o}^2 + C$$

$$0 = \frac{k_{ice}r_o}{2U} - \frac{{r_o}^2}{4} + C$$

$$C = \frac{{r_o}^2}{4} - \frac{k_{ice}r_o}{2U} \tag{29}$$

$$t = \left(\frac{\rho_{ice}L_{ice}}{k_{ice}\left(T_{freezing} - T_{coolant}\right)}\right)\left[\frac{1}{2}s^2\ln\left(\frac{s}{r_o}\right) + \frac{1}{4}\left(\frac{2k_{ice}}{r_oU} - 1\right)s^2 + \frac{{r_o}^2}{4} - \frac{k_{ice}r_o}{2U}\right]$$

$$t = \left(\frac{\rho_{ice}L_{ice}}{k_{ice}\left(T_{freezing} - T_{coolant}\right)}\right)\left[\frac{1}{2}s^2\ln\left(\frac{s}{r_o}\right) - \frac{1}{4}(s^2 - {r_o}^2)\left(1 - \frac{2k_{ice}}{r_oU}\right)\right] \tag{30}$$

The time to grow to a certain radius, s, is then as follows.

$$t = \left(\frac{\rho_{ice}L_{ice}}{k_{ice}\left(T_{freezing} - T_{coolant}\right)}\right)\left[\frac{1}{2}s^2\ln\left(\frac{s}{r_o}\right) - \frac{1}{4}(s^2 - {r_o}^2)\left(1 - \frac{2k_{ice}}{r_o\left[\frac{D_{outer\ tube}}{D_{inner\ tube}h_{inner}} + \frac{D_{outer\ tube} * \ln\left(\frac{R_{outer\ tube}}{R_{Inner\ tube}}\right)}{2k_{tube}}\right]^{-1}}\right)\right] \tag{31}$$

This final equation, derived in detail is similar to that as reported in Bejan's Heat Transfer Handbook (Bejan and Kraus, 2003), but including tube wall resistance along with inner convection.

Although the equations are exactly the same for the PCM and Ice building model the values for numerous parameters vary greatly between the two. First of all, since the two require different coolants (the ice building coolant is well below the freezing point of water, while the PCM coolant is above the freezing point of water) the inner heat transfer coefficient varies, along with the heat capacity, density, and viscosity. These physical property changes manifest themselves in a substantially lower flow rate of coolant for the ice building, because the same pump is being used. Other parameters that vary between

the two storage methods include the latent heat capacity of the two materials, their thermal conductivity, density, and most importantly, their freezing temperatures.

Convection on the outer wall of the ice is neglected here, because there is a negligible driving temperature differential between the two (See Figure 4) and by Newton's Law of Cooling, this makes the heat transfer rate negligible. The heat transfer from the inner wall manifests itself in the moving interface instead of a heat transfer into the tank.

Results

Sensible

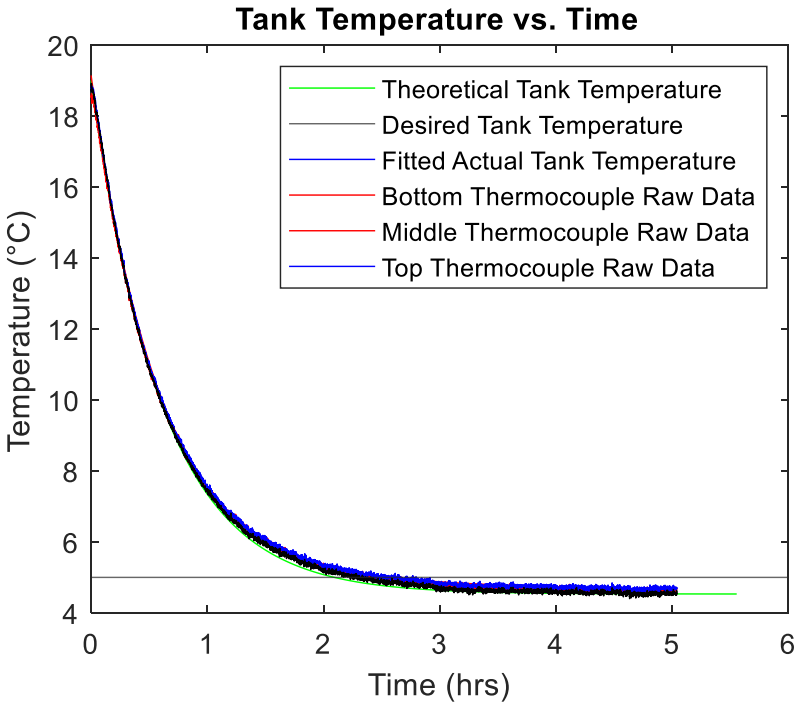

Figure 5. Water Cool Down Temperatures for Sensible Experiment

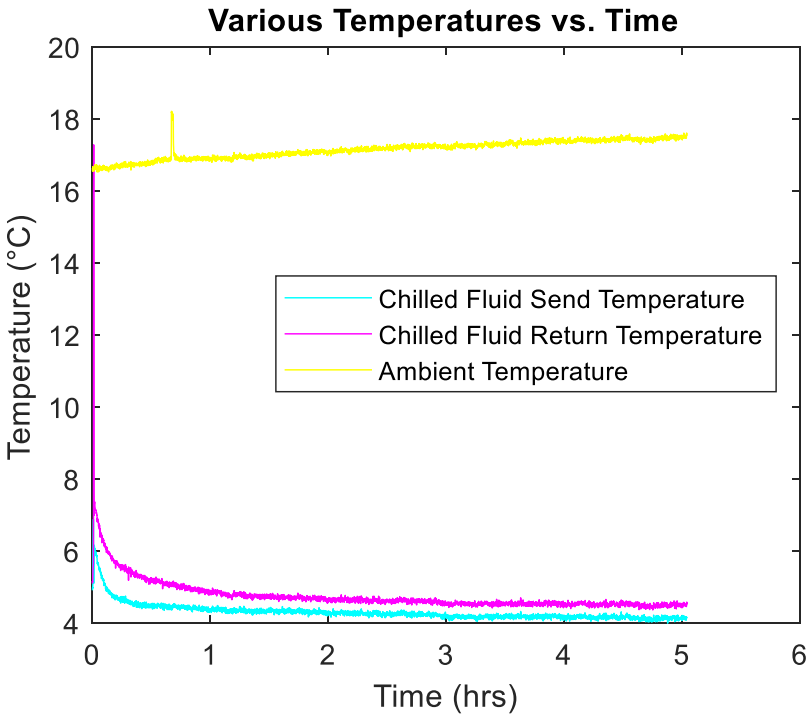

Figure 6. Ambient and Coolant Temperatures vs. Time for Sensible Experiment

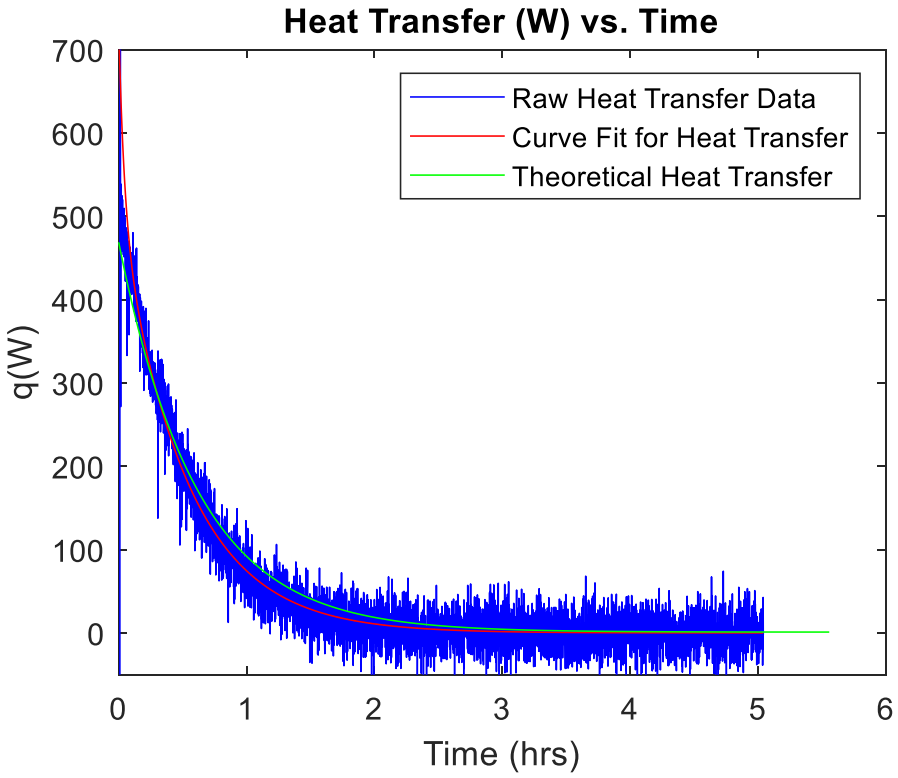

Figure 7. Heat Transfer Rate vs. Time for Sensible Experiment

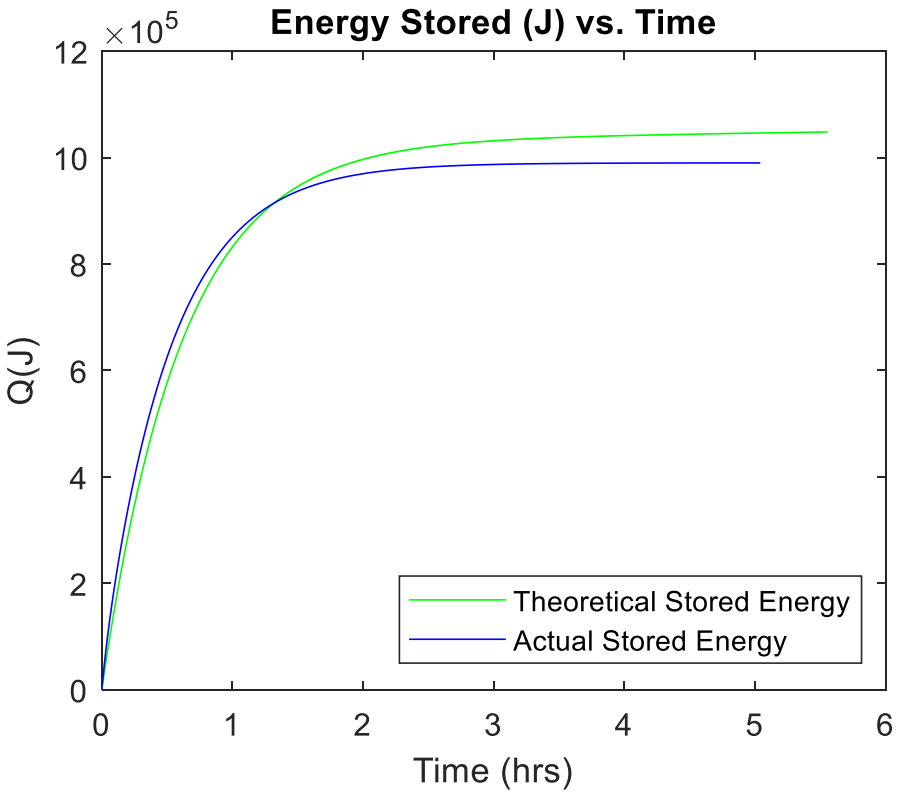

Figure 8. Energy Stored vs. Time for Sensible Experiment

Figure 5 shows the thermocouple readouts for the tank undergoing sensible cooldown. Due to the addition of the bubbler after pre-trials, there is negligible difference between the top, middle, and bottom thermocouple readouts at any given point in time, as the bubbles provide sufficient agitation to disrupt any stratification, or separation of water into layers according to density (which is a function of temperature). Although this addition of a bubbler may have contributed to the convection on the outer wall of the coil, the outer wall heat transfer coefficient was found experimentally (approximately 1000 $W/m^2 \cdot °C$) for the analytical model after this addition, so this did not contribute to error.

The curves traced in Figure 5 are standard logarithmic plots, as is expected for such a differential equation where heat transfer is a function of temperature differential between coolant and the tank, and the tank temperature varies with time according to the rate of heat transfer. At small time, said temperature differential is large and so the slope of temperature, i.e. the rate of transfer is large, and at large time the coolant and the tank are approximately the same temperature, so the slope of the temperature curve trends to zero, as the rate of heat transfer is nearly zero, save for the heat added to the tank from the environment through the insulation. It may be seen that between one and two hours, the theoretical curve trends below the actual values slightly, meaning the tank was cooling slower than expected at this point in time, but the overall agreement between predicted and measured tank temperature is excellent.

Figure 6 shows other relevant thermocouple readouts to the cooldown process. It should be noted that for the analytical model, both the coolant send temperature and ambient temperature were assumed to be constants, but for the sake of this experiment, there is obvious variation with time. For the coolant send temperature, the high rate of heat transfer at small time causes a spike in the coolant send temperature (4°C to 6°C)due to the finite volume of the chiller unit. The ambient temperature rises with time, which is likely due to the chiller unit passing heat from the tank to the finite mass of air

in the lab room through a refrigeration cycle. The logarithmic trend of the coolant return is as expected from the analytical model, and the difference between the coolant inlet and return at large time is attributed to the heat gain of the tank from ambient; applying the first law of thermodynamics (i.e. $q = \dot{m}C_p\Delta T$), there is a mass flow rate of coolant through the coil, and the temperature rise of that coolant from inlet to outlet therefore depends on its value of specific heat.

Figure 7 shows the raw data for the heat transfer of the sensible experiment, as a function of the temperature difference between coolant in and out, using the first law of thermodynamics, as mentioned in the previous paragraph. Because this is noisy data, a trend line is applied in red, to compare to the theoretical heat transfer (green) from the analytical model. Between half an hour and two hours, the actual heat transfer is slightly below the theoretical model, but match thereafter.

It may be noted that the same heat transfer behavior found in Figure 7 could alternatively be found by applying the first law of thermodynamics to the derivative of the tank temperature curve with respect to time, here using the mass and specific heat of the storage media in the tank (in this case water).

By simply integrating the heat transfer curves of Figure 7 with respect to time, Figure 8 then displays the energy stored in the sensible experiment as a function of time. The discrepancy between the actual and theoretical heat transfers between half an hour and two hours manifests itself here as a shift in final energy that the tank asymptotically approach. The actual total amount of energy stored in tank water, sensibly, for this specific test vessel was 1,198,673 Joules.

For the sake of this sensible trial and both subsequent latent trials for ice and PCM, coil tube and plastic bucket heat capacity were not included in total capacity (J) calculation and plots shown, but was approximately the same for all three technologies tested (save for the slightly different temperature differentials from start to finish). The tube and bucket heat capacity would be highest in relation to the

media heat capacity for this sensible case (since this media has the lowest final “charged” energy), and even in this case the energy stored in the tube and bucket is only 2.72% of that stored in the water.

Latent (Ice)

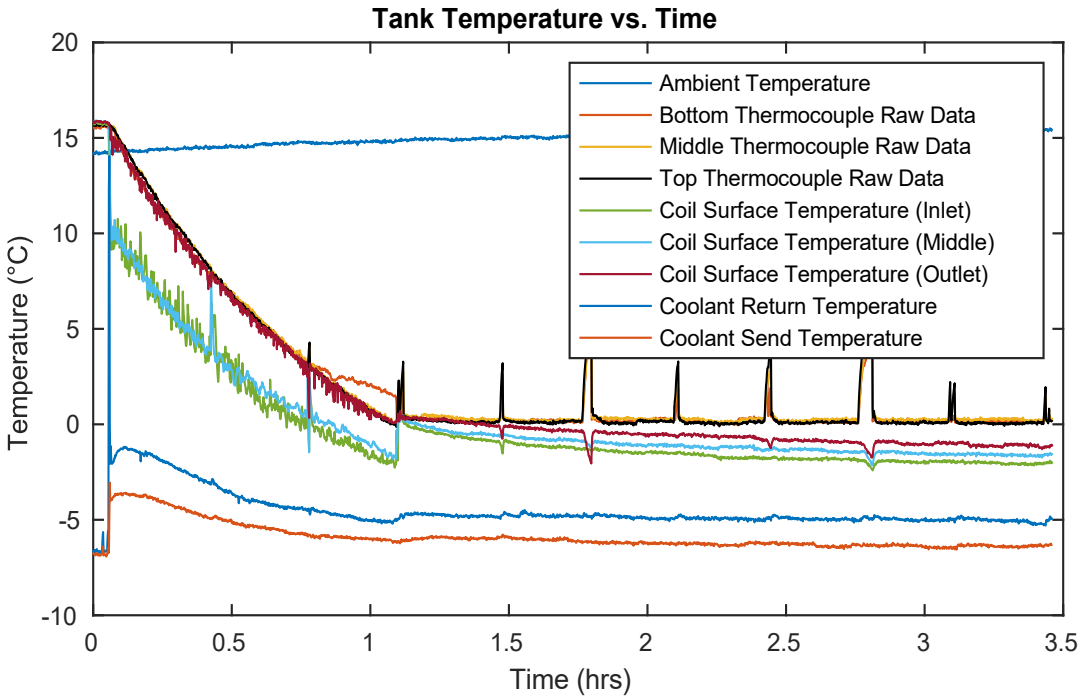

Figure 9. Ice Storage Temperatures vs. Time at Various Locations, Coolant Temperatures, Ambient Temperatures

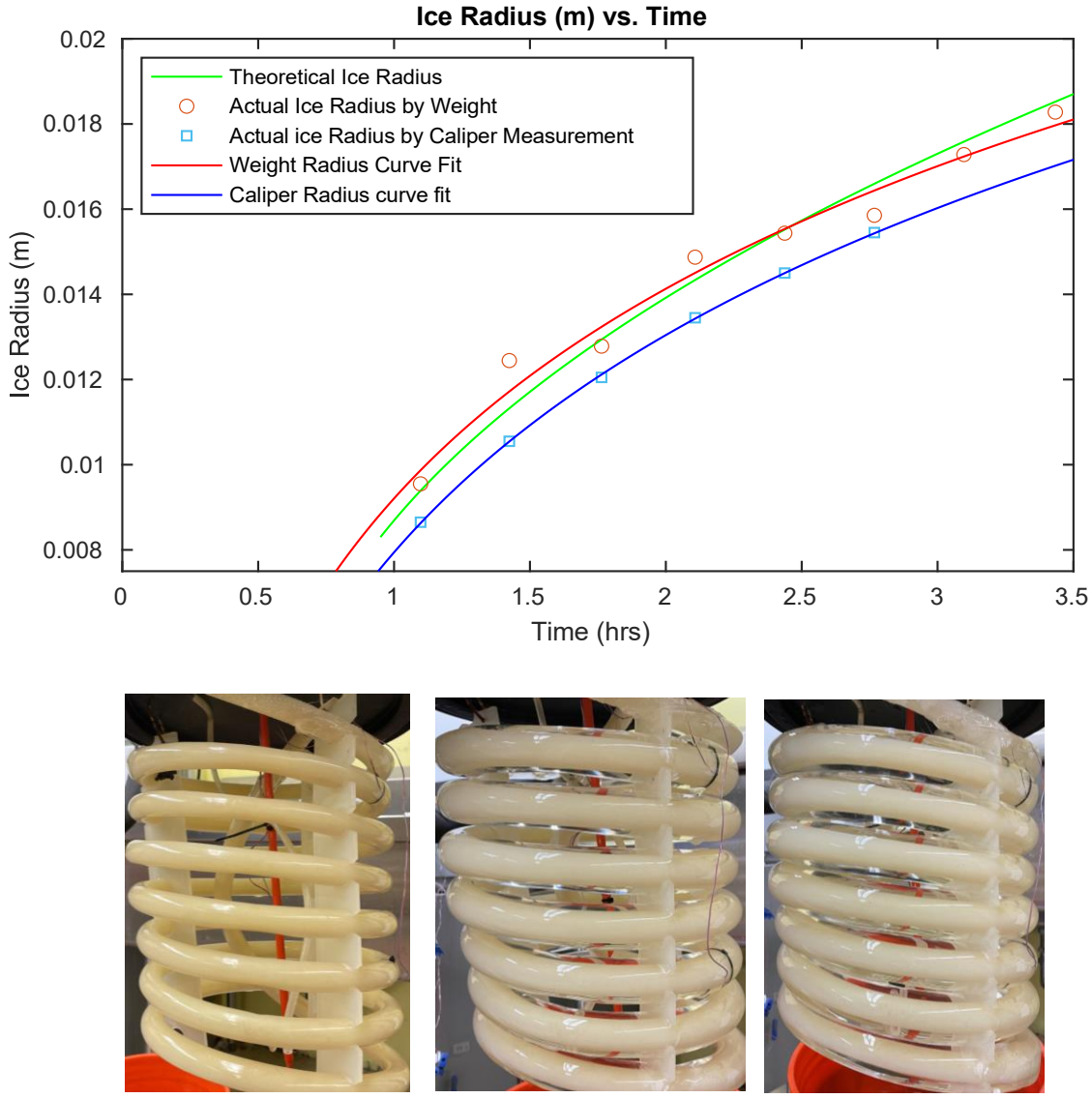

Figure 10. Ice Radius vs. Time for Latent (Ice) Experiment and Representative Ice Building Photos at Time = 1:05, 2:25, and 3:25 hours

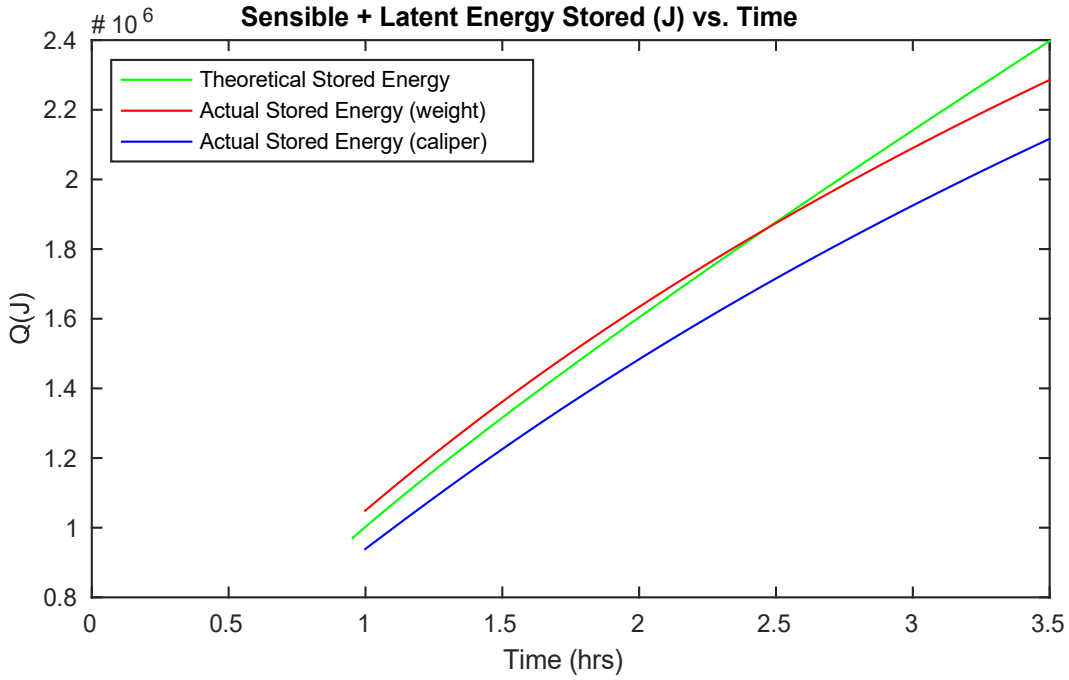

Figure 11. Total Energy Stored in Ice Building

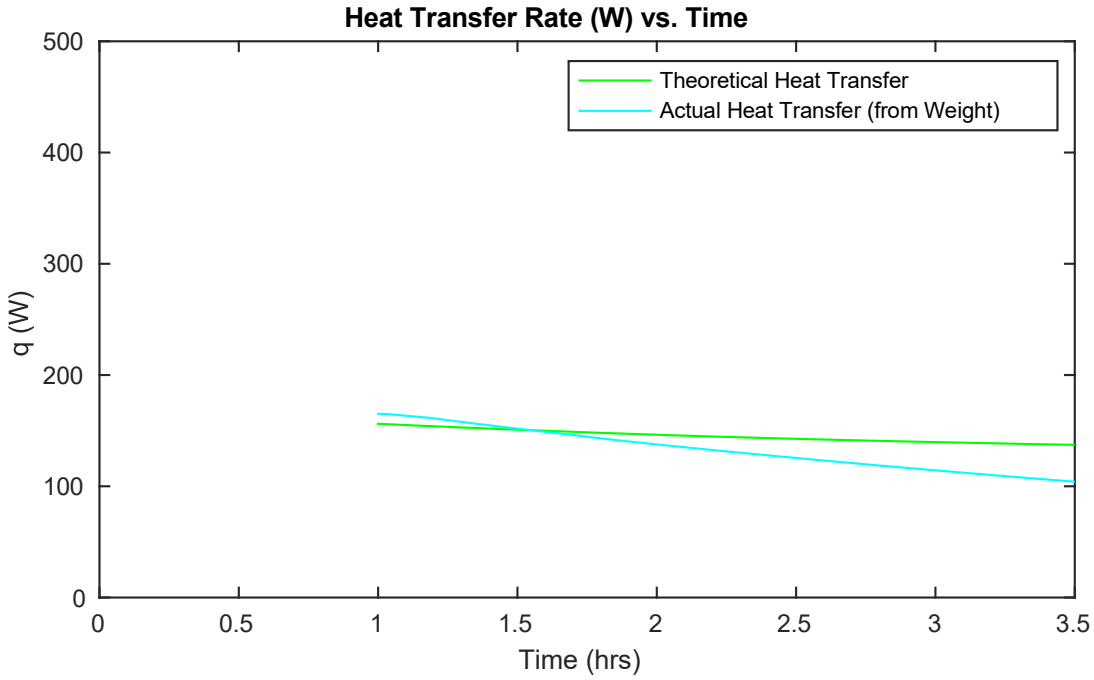

Figure 12. Heat Transfer Rate vs. Time During Ice Building

Figure 9 shows temperatures at various locations in the system throughout the water cooldown and ice building run. Sensible cooling of the tank water occurs from time t=0 to t=1 hr, after which ice building begins. It may be noted that the coolant send temperature as well as the ambient temperature are not perfectly constant with respect to time as the theoretical model assumes, and just like the sensible run, this is due to the finite chiller reservoir volume and the heat the chiller puts into the lab room through its refrigeration cycle. It also may be seen that the coil surface temperature momentarily dips below 0°C, the freezing point of water, just after one hour. This is due to the fact that water may sub-cool several degrees before initial nucleation of ice occurs, at which point the temperature suddenly returns to the normal freezing point of water. All three of the center rake thermocouples trend nicely at the freezing point of water after the sensible portion, as would be expected, but the periodic spikes are a result of pulling the coil out of the vessel for measurement of the ice layer radius. Noting that the three coil surface temperature measurements trend downward for the duration of the freezing, the use of a convection inner boundary in the analytical model is justified; if there was a constant temperature boundary condition, these temperatures would be horizontal lines. The coil surface temperatures are always below the tank center rake temperatures, as they are closer to the coolant (which is below the freezing point of water).

Figure 10 shows the theoretical ice radius as predicted using the theoretical Stefan solution, the actual average ice radius determined by direct measurement at three locations in the tank using calipers at regular intervals, and a calculated ice radius from a hanging scale weight measurement of the coil. Trend lines have been added to the data points of the two radius measurement methods, and it may be noted that at higher time, there are no longer data point for the caliper-based measurement. This is due to the fact that the ice had linked or nearly linked between the helically wound coils, prohibiting caliper measurement. The photographs included in Figure 10 depict ice building soon after nucleation (1:05),

partway through building (2:25), and at linkage (3:35). For small time, the theoretical ice radius falls between the weight-based and caliper-based measurements, but at large time, both measured curves fall below the theory. This is likely due to but air inclusions decreasing the ice thermal conductivity, as well as the removing of the coil from the tank to measure the ice radius, which would expose the coil and the chilled tank water to convection and radiation to the environment.

Figure 11 shows the total energy stored in the ice building process, which is more than two million joules in just over two hours time once freezing is initialized. The total latent energy stored is found as a function of time, since the volume of ice is a function of the ice radius, the volume is related to a mass with the density of ice, and that mass then multiplied by the latent heat of freezing for water. The latent energy is shifted up by the amount of sensible energy storage required to get the tank from the starting temperature to the freezing point, using the first law of thermodynamics. This sensible cool down period could have been modeled using the same equations as used in the sensible cool down section, but for the sake of brevity, is disregarded here. The predicted model for stored energy falls neatly between the two actual energy stored curves, but surpasses even the weight-calculated curve at large time. As explained previously, this may be attributed to the thermal conductivity of the ice being lower than expected, due to inclusion of air bubbles, as well as the periodic exposure of the ice to the lab temperature to probe the radius.

Figure 12 shows the heat transfer rate [W] for only the latent storage portion of the Ice storage cool down. This is found simply as the derivative of the latent energy heat transfer curve of Figure 11. It may be noted that the theoretical heat transfer rate decreases with time due to the ice layers increasing resistance (a function of thickness), but the actual rate started out somewhat higher before crossing over and dropping below the theoretical value after 1.5 hours.

Latent (PCM)

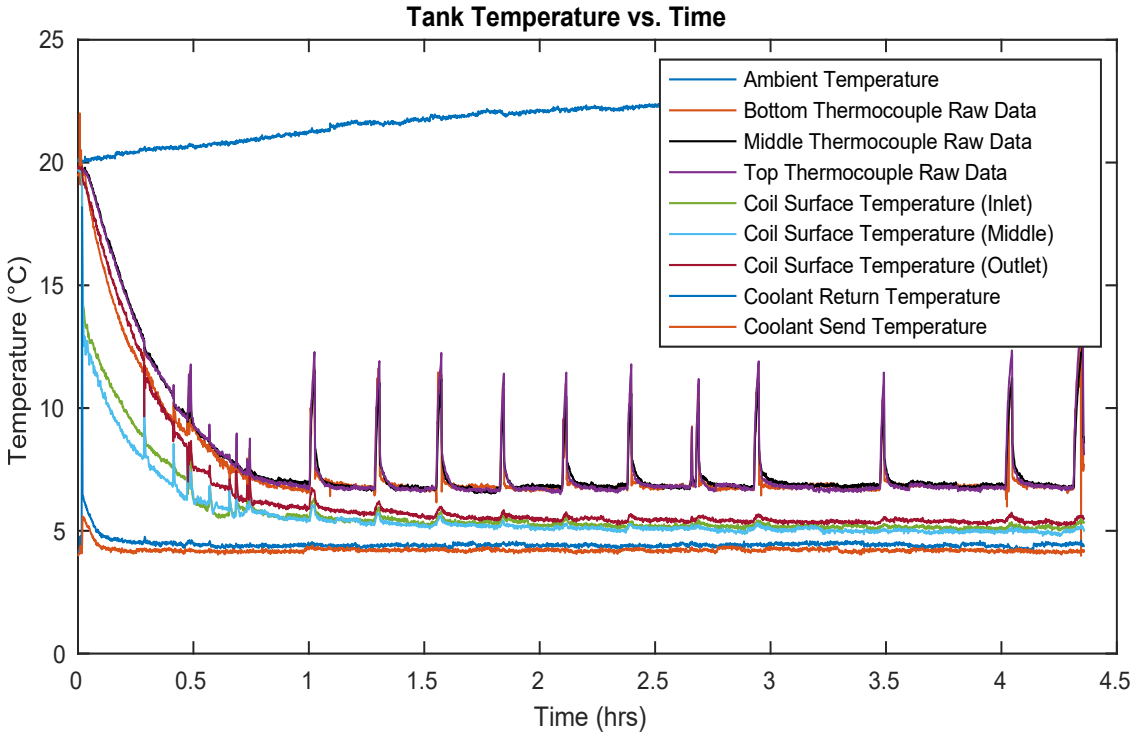

Figure 13. Tank Temperatures, Coolant Temperatures, and Ambient Temperature vs. Time for PCM Experiment

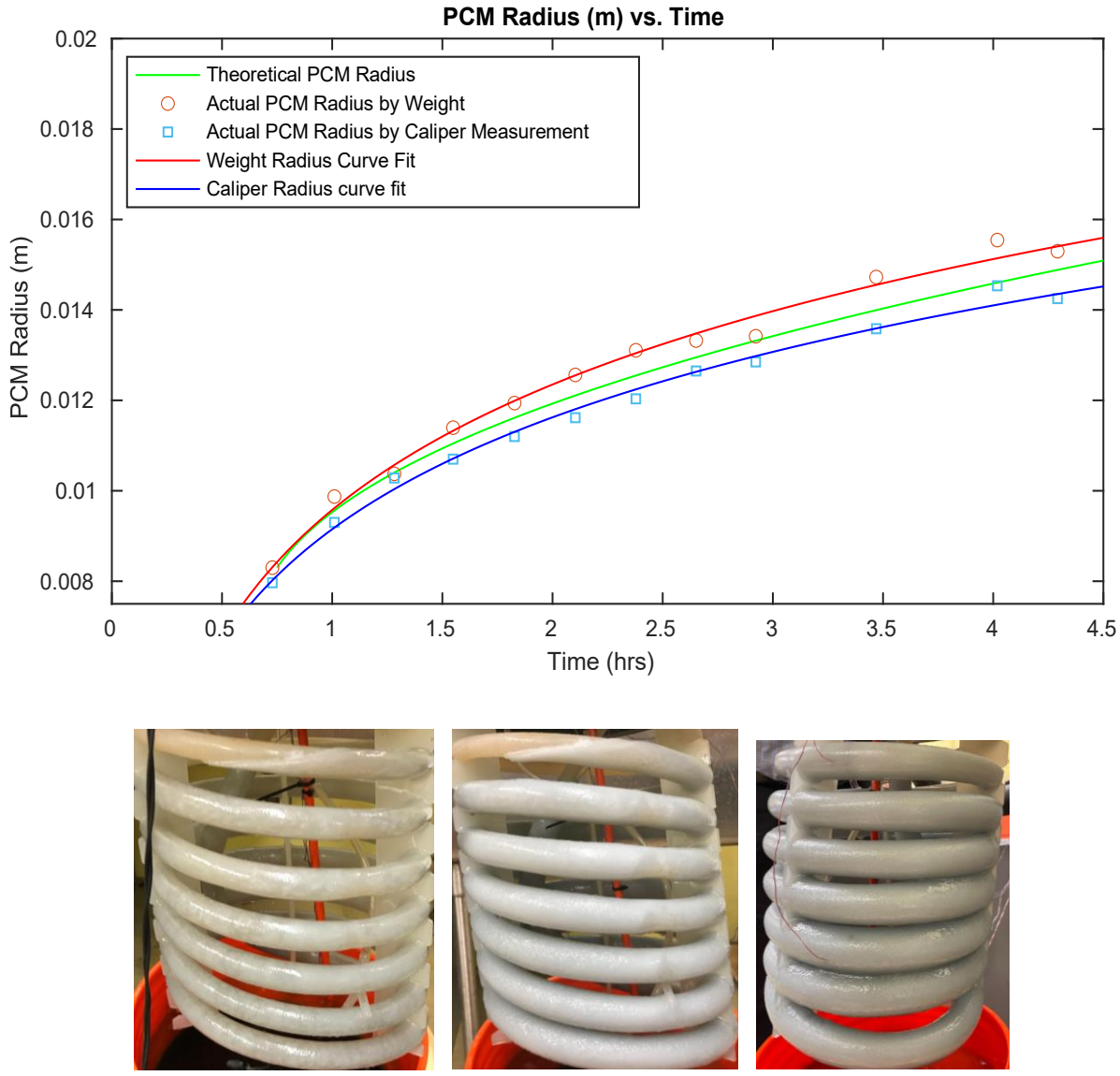

Figure 14. Frozen PCM Radius vs. Time for Latent (PCM) Experiment and Representative PCM Solidification Photos at Time = 1:20, 2:20, and 4:20 hours

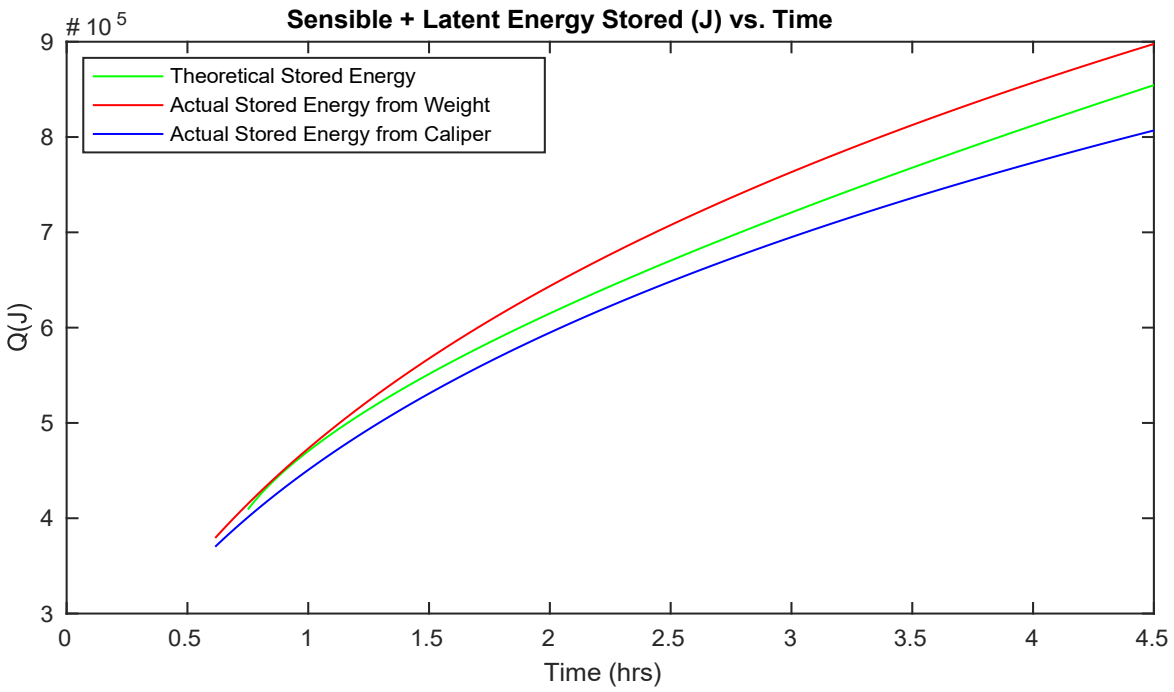

Figure 15. Total Energy Stored in PCM vs. Time

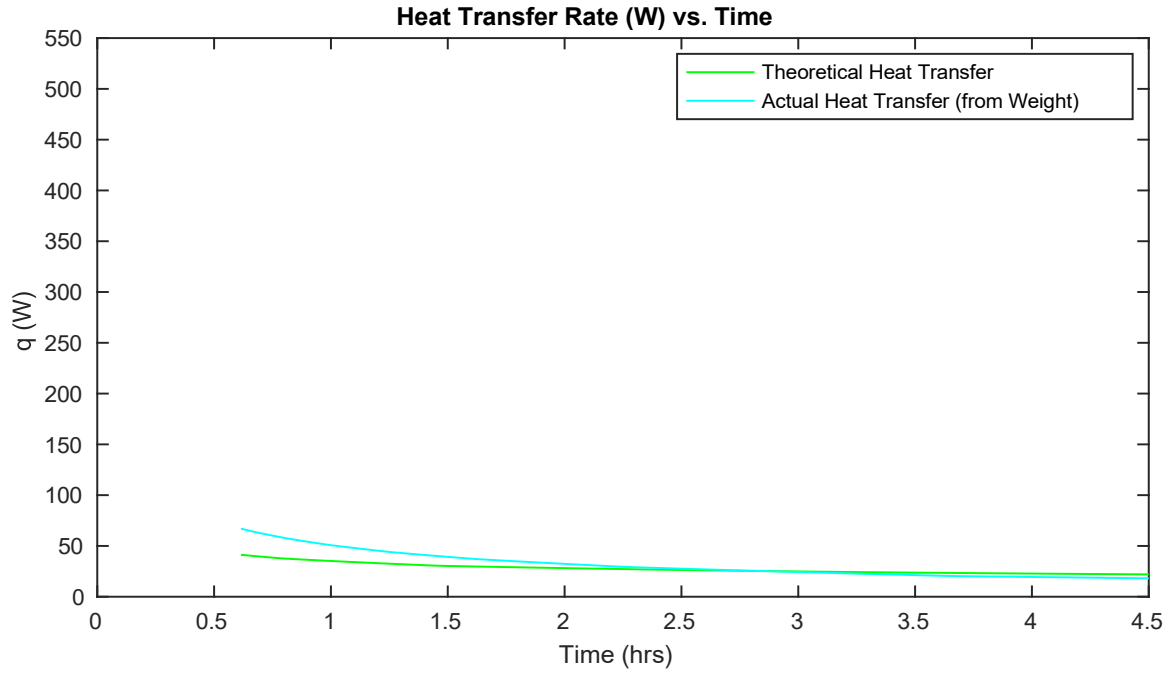

Figure 16. Heat Transfer Rate vs. Time during PCM Freezing

Figure 13 shows all thermocouple read outs for the PCM tank over time. Here again it is seen that at very small time, the coolant send temperature spikes due to the finite volume of the chiller reservoir. The ambient temperature also drifts upward, likely due to the heat input to the lab from the chiller refrigeration cycle. Unlike the Ice building, the PCM here does not sub-cool before nucleation of frozen media occurs, but rather goes directly from sensible cooling to latent freezing after approximately 3/4 an hour. The spikes in temperature seen on the tank center thermocouple rake are done at regular intervals for the first eight measurements, then the interval is doubled for two measurements so as to minimize disturbance to the slowing build rate, and then for the final measurement it is returned to the initial interval for the final measurement. Much like the ice experiment, the center rake remains at the freezing point of the media (PCM here) while the coil surface thermocouples record subfreezing temperatures.

Similar to that shown for the latent ice building in Figure 10, Figure 14 shows the theoretical frozen PCM radius as predicted by the Stefan solution, as well as data points calculated from weight and diameter measurement (by caliper). Once again, trend lines are added to the data points for comparison to the theoretical curve. Here, however, the theoretical curve falls between the weight-based and caliper-based radius measurement for the full duration of the trial. Over the four and a half hours that the trial was conducted linkage was not achieved. The photos in Figure 14 depict the frozen PCM on the coil at times 1:20, 2:20, and 4:20.

Total Energy stored in theory and by actual measurements, all as a function of time, are shown in Figure 15. The curve itself is therefore that of the latent storage, and shifted up in magnitude by the sensible energy stored in the process of bringing the tank from the initial temperature to the freezing point of the PCM. Once again, the PCM sensible cool down rate could be predicted using the same equations as the sensible water cool down (using the thermophysical properties of PCM), but this is omitted in this section to focus on the latent PCM freezing portion.

Figure 16 shows that the actual heat transfer rate starts out moderately higher than the theoretical value, but then converges with that value at large time. It may be noted that the heat transfer rate is lower than that of water's latent cooling to ice, as the driving temperature differential between the freezing point (tank temperature) and coolant temperature is substantially smaller here.

Comparison of Different Technologies

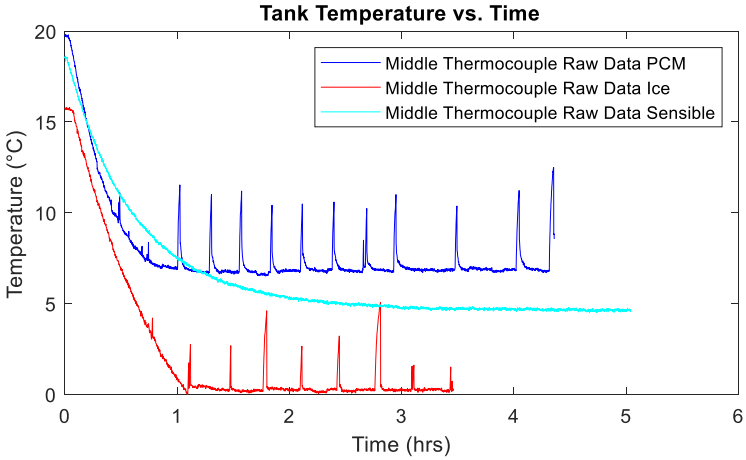

A .Comparison of Middle Thermocouple Data for All Three TES Techniques

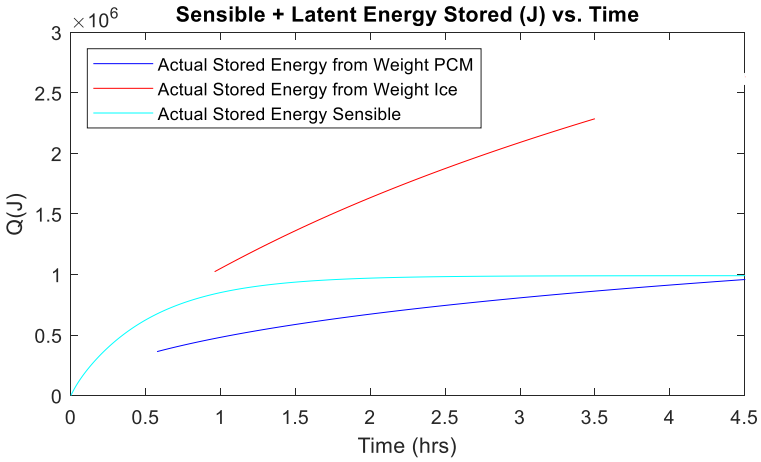

B. Comparison of Total Energy (Sensible and Latent) Stored in Each of The Three Techniques

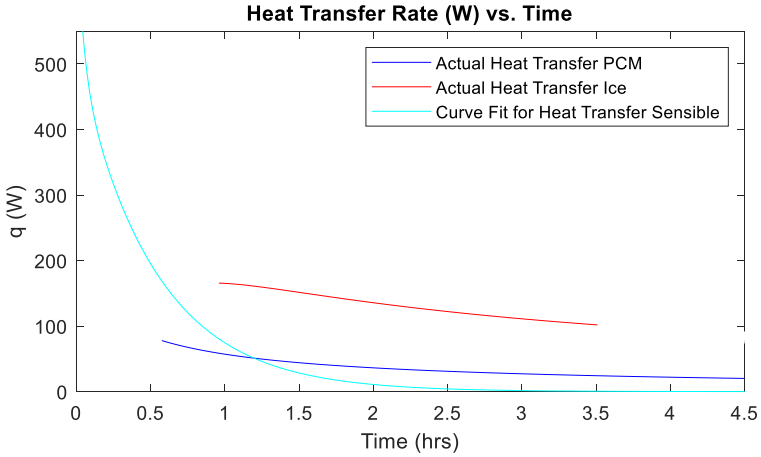

C. Heat Transfer Rate for Each of the Three Thermal Energy Storage Techniques

Figure 17. Comparison of the Three TES Technologies

Figure 17 shows a comparison of the three technologies, as superimposed on the same plots. Figure 17A shows the middle temperature on the thermocouple rake with respect to time. Here, it is seen that the temperature of the sensible decreases logarithmically toward the coolant chiller temperature, reaching the steady-state asymptote after three hours. The curves for PCM and ice building are not so smooth, for two main reasons. One is that they abruptly halt their sensible cooldown when they reach their freezing point, the other being that the measured values required removal of the coil from the tank. Since the center thermocouple rake did not have any ice or frozen PCM on it, it had no insulation to ambient on these removals, resulting in spikes. It should be noted that the middle thermocouples are at the freezing point of their respective medias after the initial sensible cooldown of the liquid is complete. If there was a substantially longer cool down period, and no heat gain from the lab environment, the center thermocouple rake would freeze into the mass of ice, and then experience a second sensible cooldown period of the solid ice or PCM.

Figure 17B shows the comparison of the energy storage for each of the methods. For sensible, the rate of energy increase is largest when the tank temperature is highest, and then once the tank temperature becomes the temperature of the cooling fluid, the energy plateaus to a steady value. For PCM and Ice, the energy storage increase continues for the duration of the trial, as neither of the tanks reaches the coolant temperature (they would need to completely freeze and then sensibly sub-cool to do such). It may be noted though, that the energy stored for ice, and the rate at which it stored is higher than PCM, which may be attributed to the higher driving temperature differential between the coolant and the freezing point of water, the higher thermal conductivity of water ice, and due to the larger latent heat of fusion value. At the end of four and a half hours, the PCM has not reached the energy storage level of sensible chilled water, but would at larger time. At the four and a half hour mark, ice has more than double the stored energy of the other two.

Since the heat transfer rate is the derivative of the energy stored, Figure 17C follows directly from Figure 17B. Here, as expected, the heat transfer rate for sensible is largest at the beginning when the temperature differential between coolant and tank water is greatest, and then reaches almost zero (save for tank heat gain) at large time. For ICE and PCM, the sensible heat transfer curves would have looked similar to that of the sensible run, and once they start freezing (where they start on the plots), it is seen that their respective heat transfer rates decrease gradually, as the ice and PCM layers serve to insulate the coil from the tank fluid. Once again, since the ice has a larger temperature differential and higher thermal conductivity, the heat transfer rate is substantially higher than that for PCM.

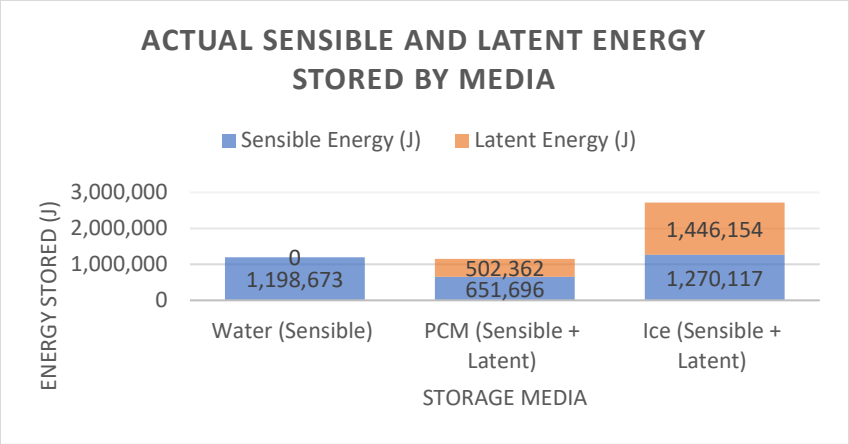

A. Actual Sensible Storage Comparison

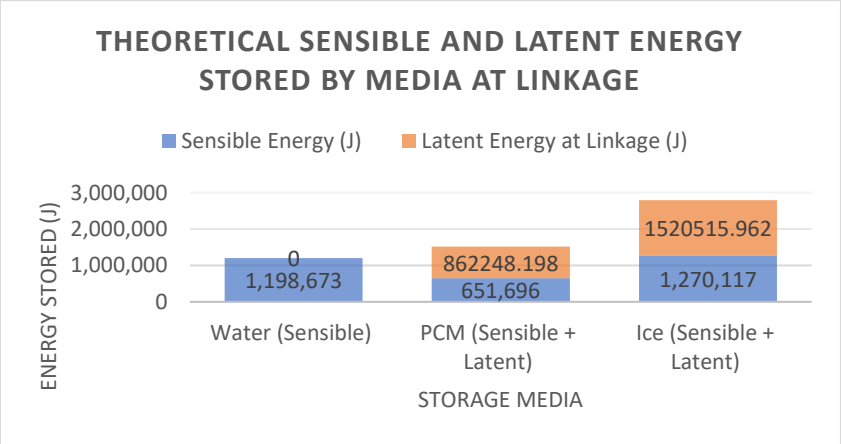

B. Theoretical Storage for at Linkage (For the Two Latent Cases)

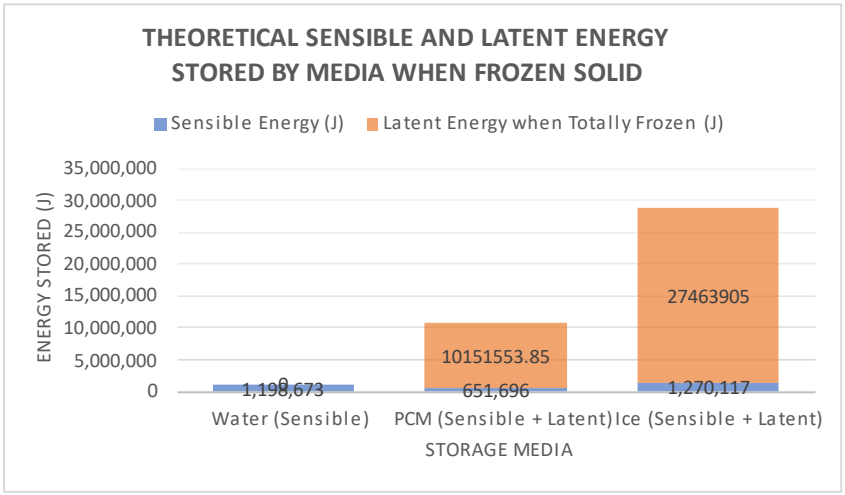

C. Theoretical Storage if Latent Media Freezes Solid

Figure 18. Comparison of Actual and Theoretical Energy Stored for the Three TES Technologies

Figure 18A shows the achieved storage amounts of energy for the experimental runs. Here it is seen that the sensible and PCM both achieved approximately the same total storage amount in the duration the experiment lasted for (although sensible took only two hours to charge vs. 4.5 for the PCM), and the ice stored more than double (but also requiring a 4.5 hour charge). It should be noted that the sensible portion of the PCM cooldown is substantially lower than that of water (651,696 J vs 1,198,673, respectively) due to PCM's substantially lower specific heat.

Figure 18B shows the energy stored if the PCM frozen on the coils was allowed to link, or converge in the middle of the coil gaps (recalling that PCM did not achieve the radius that ice did). Such linkage would be achievable running the experiment longer, but even with this linkage, the amount of energy stored in PCM is not significantly higher than the sensible run, but if the coils occupied a higher percentage of the tank volume (as they do in industrial units) then the difference would be more substantial, which will be discussed next.

Figure 18C shows this extreme case, if all of the storage media froze solid in the tank. Here it is seen that sensible storage pales in comparison to the other two. Such a case would be feasible with a coil configuration that occupied a larger percentage of the tank (while maintaining even spacing), as mentioned above, although for a fixed tank volume, such a coil would also occupy more volume itself, and therefor decrease the storage amount from that in Figure 18C.

Conclusions

For the purposes of thermal energy storage, a number of conclusions may be drawn from the analytical and experimental results of this thesis. These conclusions are especially valuable in their ability to provide a more nuanced view of the three major storage techniques in terms of practicality than basic thermodynamics might.

Water as a sensible storage media, when viewed from a thermodynamic point of view, seems to pale in comparison to the other techniques, as the sensible energy it may store is an order of magnitude smaller than the latent energy of the two freezing techniques. However, by modelling the actual cool down process analytically and experimentally, what is found is that when the cooling temp is approximately the temperature of a common HVAC evaporator coil, the cool down occurs rapidly due to the high convection heat transfer coefficient and high thermal conductivity of water. Because of this, a large volume of water may be chilled in the four to six hour typical off-peak cool down period with a relatively small heat exchanger or coil.

Phase Change Material (specifically Puretemp 8, in this thesis), on paper, may seem to be an ideal candidate for a storage media; it freezes at temperatures efficiently achieved with common HVAC condensing units, once frozen it has energy storage on the same order of magnitude as frozen water, and because of its high energy density, its vessels may be relatively small. Upon completion of the analytical and experimental research, however, this material shows some major issues. In part due to the small driving temperature differential between chiller (at common HVAC temperature) and the freezing point of the material, and in part due to the very low thermal conductivity of the frozen material, this material is the slowest to

freeze. This issue could be mitigated by having a lower chiller temperature, or higher freezing point PCM, but doing either would defeat the main purposes of this material. First, changing the PCM to one with a higher freezing point would mean an inefficient discharge, because then the liquid used to melt the PCM (and cool the air using an air to water heat exchanger) would then have less of a driving temperature differential between itself and the facility air. Second, each condensing unit in a refrigeration system has a specific range of temperatures it is designed and charged with freon for, and lowering the evaporator temperature decreases its efficiency. A new unit could be purchased to optimize efficiency for said lower temperature, but if a new unit is being selected, it could just as easily be one capable of building water ice, which, as a media, costs orders of magnitude less and performs better in many ways, as has been shown in this study.

Frozen water, although requiring a lower temperature chiller, outperformed the other methods in many ways. In four and a half hours time, the ice on the coil had linked, and in doing so stored more than double what the other two methods were able to achieve. This was, in part, due to the large temperature differential between the coolant mixture and the tank water, made possible by chiller at lower than typical-HVAC temperatures. This was also due to ice having a higher thermal conductivity than its PCM counterpart. While the lower temperature refrigerant condensing unit is an added cost, this method benefits from the low cost of storage media (regular water) just as the sensible did, but also from the much lower volume storage vessel as compared to the sensible cooling, which is expected from a media undergoing latent cooling.

Overall, for sensible and latent storage in three separate techniques, the experimental and theoretical models (using sensible cooldown and Stefan solutions) fit extremely well in this thesis. This combination of theoretical and experimental models offers much more than a purely

theoretical or purely experimental thesis, and is even more useful due to the careful selection of temperatures chosen, to make this thesis useful to actual HVAC applications, instead of merely hypothetical lab experiments.

References

Bejan, A. and Kraus, A.D., *Heat Transfer Handbook*. New York: Wiley, 2003. Chapter 3.10, pp. 243-253.

Caldwell, J. and Chiu, C.K. *Numerical solution of one-phase Stefan problems by the heat balance integral method, Part I—cylindrical and spherical geometries*. Commun. Numer. Meth. Engng., 16: 2000, pp. 569-583.

Chen, S-L. and Lee, T-S., *A study of supercooling phenomenon and freezing probability of water inside horizontal cylinders*, International Journal of Heat and Mass Transfer, Volume 41, Issues 4–5, 1998, pp. 769-783.

Coleman, H. and Steele, W., *Experimentation and Uncertainty Analysis for Engineers*. New York, Wiley, 1989.

Cummings, M. S. *Modeling, Design, and Control of Partial Ice-Storage Air-Conditioning Systems*. M.S. Thesis. *University of Wisconsin-Madison* , 1989.

Intemann, P. A. and Kazmierczak, M. J., *Heat transfer and ice formations deposited upon cold tube bundles immersed in flowing water—I, Convection Analysis*, International Journal of Heat and Mass Transfer, Volume 40, Issue 3, 1997, pp. 557-572.

Jekel, T.B., Mitchell J.W., and Klein S.A. 1993. *Modeling of Ice-storage tanks.* ASHRAE *Transactions*: Symposia, CH-93-10-2.

Kazmierczak, M. J. and Nirmalanandhan, V., *Heat transfer augmentation for external ice-on-tube TES systems using porous copper mesh to increase volumetric ice production*, International Journal of Refrigeration, Volume 29, Issue 6, 2006, pp. 1020-1033.

Khalid, M.Z., Zubair, M., and Ali, M. *An analytical method for the solution of two phase Stefan problem in cylindrical geometry*, Applied Mathematics and Computation, Volume 342, 2019, pp. 295-308.

Lindsay, B., Andrepont, J.S., *Evolution of Thermal Energy Storage for Cooling Applications*, *ASHRAE Journal*, October 2019, pp. 42-59.

Manlapaz, R. L. and Churchill, S.W., *Fully Developed Laminar Convection From a helical Coil*, Chemical Engineering Communications, 9:1-6, 1981 pp. 185-200.

Mehling, H. and Cabeza, L. F. *Heat and Cold Storage with PCM - An up to Date Introduction into Basics and Applications*. Berlin, Germany: Springer, 2008.

Pereira da Cunha, J. and Eames, P., *Thermal energy storage for low and medium temperature applications using phase change materials – A review*, Applied Energy, Volume 177, 2016, pp. 227-238.

Schafer, K. *Stratified Laboratory Thermal Energy Storage (LabTES) Tank Experiments: Sensible Only and Sensible Augmented with PCM-Filled Tubes*. M.S. Thesis. University of Cincinnati, 2016.

Wildin, M.W., Mackie, E. I., and Harrison, W.E., *Stratified Thermal Storage. A new/old Technology. ASHRAE Journal*, vol. 32, no. 4, 1990, pp. 29-40.

Yener, Y. and Kakaç, S. *Heat Conduction*. 4th ed. New York, Taylor & Francis, Chapter II, 2008.

Appendix A: Stefan Number Calculation

The Stefan number is the ratio of sensible heat to latent heat. Its equation is as follows.

$$St = \frac{c_p \Delta T}{L} \tag{32}$$

Where c_p is the sensible heat (for solid phase ice or PCM for the case of freezing), ΔT is the Temperature differential between the inner cooling wall and the tank temperature (at freezing point of the material), and L is the Latent heat of freezing for the material.

When the sensible heat is substantially smaller than the latent heat (St < 0.1) the quasi-steady approximation applies (Mehling and Cabeza, 2008).

For Ice Experiment:

$$c_p = 4{,}186\, J/kg°\text{C}$$

Since the largest temperature differential occurs at large time at the inlet of the coil, this temperature shall be used to conservatively estimate the Stefan number.

$$\Delta T = \ 0 - (-2.14°\text{C}) = 2.14°\text{C}$$

The latent heat of water freezing is then,

$$L = 334{,}000\, J/kg$$

$$St = \frac{4{,}186 \frac{J}{kg°\text{C}}\ (2.14°\text{C})}{334{,}000\, J/kg}$$

$$St = 0.0268$$

For PCM Experiment:

$$c_p = 1{,}850\, J/kg℃$$

Since the largest temperature differential occurs at large time at the inlet of the coil, this temperature shall be used to conservatively estimate the Stefan number.

$$\Delta T = 8 - (4.96℃) = 3.04℃$$

The latent heat of water freezing is then,

$$L = 178{,}000\, J/kg$$

$$St = \frac{1{,}850 \frac{J}{kg℃}\ (3.04℃)}{178{,}000\, J/kg}$$

$$St = 0.0315$$

Appendix B: Nusselt Number Calculation and Comparison to Straight Tube

The Nusselt Number for the inner surface of a helical coil is described by a correlation developed by Manlapaz and Churchill using a compilation of experimental data, as follows (Manlapaz and Churchill, 1981).

$$Nu_T = \left[\left(3.657 + \frac{4.343}{x_1}\right) + 1.158\left(\frac{De}{x_2}\right)^{3/2}\right]^{1/3} \tag{33}$$

Here,

$$x_1 = \left(1.0 + \frac{957}{De^2 Pr}\right)^2$$

And,

$$x_1 = 1.0 + \frac{0.477}{Pr}$$

Where De, the Dean Number, is a non-dimensional value relating the viscous and centrifugal forces acting upon a flow, as follows.

$$De = Re\sqrt{\frac{d}{D}} \tag{34}$$

Where d is the inner tube diameter, and D is the helix diameter.

The Manlapaz-Churchill correlation is good for all Reynolds numbers, as it was derived from a compilation of multiple helical coil studies which had Reynolds (as well as Dean and Prandtl numbers) spanning a very large range. It may be noted that as the Manlapaz-Churchill correlation trends toward Re=0, it approaches the Nusselt number for laminar pipe flow (3.66). The Manlapaz-Churchill correlation is usually presented with the Dean number as the x-axis, but for the sake of the plot in Figure 19, the Dean number was divided by the square root of the quotient tube diameter over helix diameter (which

is unique to the specific experimental setup conveyed in this paper) so that the correlation could be compared to the straight tube relations.

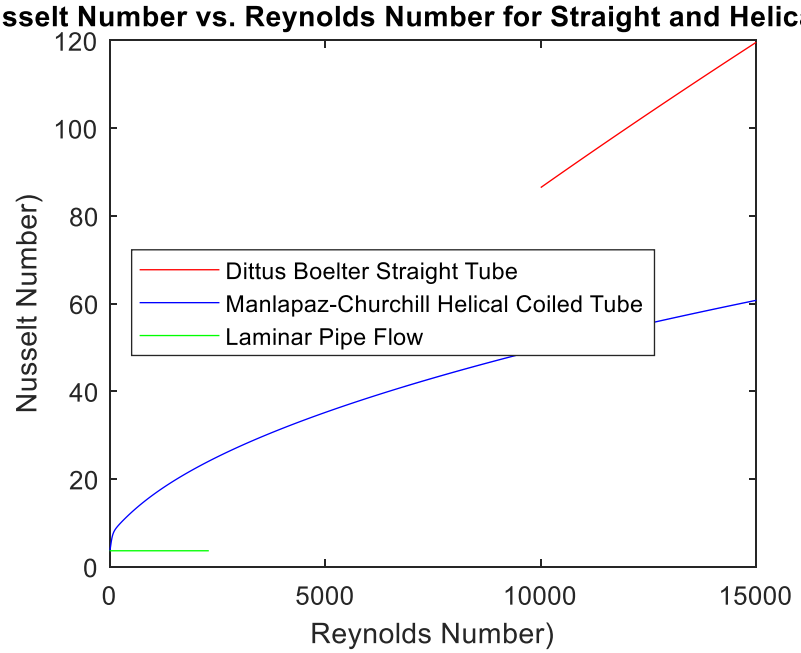

Figure 19. Nusselt Number vs. Reynolds Number at Pr = 8.66 Helical Coil vs. Straight Tube

As Figure 19 demonstrates, for the given range of Reynolds Numbers, the helical tube values fall in between the laminar and turbulent flow relations for straight tubes. They are higher than laminar flow due to a thinner wall boundary layer (due to swirl) and less than the turbulent case since helical tube forces the flow to remain laminar to higher Reynolds Numbers while the straight tube becomes turbulent flow at much lower Reynolds Numbers (Manlapaz and Churchill, 1981). All other variables held constant, these Nusselt numbers are directly proportional to the heat transfer coefficient experienced on the inner wall of the tube. For the sake of this experiment, all trials are run with the same helical tube, with helix diameter 0.2421m, and inner tube diameter 0.0127m.

Table 3. Inner Heat Transfer Coefficient for Helical Coil at Various Flow Rates

GPM	Reynolds Number	Nusselt Number	Heat Transfer Coefficient (W/m^2K)	Coolant
0.25	1306	18.4508	849.9051	Water
0.5	2612	25.6086	1179.6	Water
0.75	3918	31.2122	1437.7	Water
0.91 (Ice)	1251.2	18.1959	1080.3	70% Water 30% Ethylene Glycol (By Mass)
1	5224	35.9668	1656.7	Water
1.50 (PCM)	7836.1	43.9733	2025.6	Water
2	10448	50.7388	2337.2	Water
2.19 (Sensible)	11441	53.085	2445.3	Water
3	15672	62.1036	2860.7	Water

Appendix C: Uncertainty Analysis

For Thermocouples:

The uncertainty for the thermocouple measurement is determined using the following equation.

$$U_{T(℃)} = \frac{U_V}{SMJ} \tag{35}$$

Here U_T(°C) is the equivalent temperature uncertainty, U_V is the voltage measurement uncertainty (a property of the data acquisition unit), and SMJ is the thermocouple sensitivity at the measuring junction temperature. For Omega Fine Gauge Duplex Type-T Thermocouple Wire Tolerance Class 1, using Omega OMB-DAQ-56 USB Data Acquisition unit [0.015% of reading +0.002% of range (k=2)], at 7°C, T-type thermocouples give 0.273 mV, (0.002mV/*C *0.5°C sensitivity), with a voltage range of T-type= -6.258mV to 20.872mV, the calculation is as follows.

$$U_V = \frac{0.015 \times \left(\frac{0.273}{100}\right) + 0.000542mV}{2}$$

$$U_V = \pm 0.000291mV$$

$$U_{T(℃)} = \frac{\pm 0.000291mV}{\pm 0.001 \frac{mV}{℃}}$$

$$U_{T(℃)} = 0.291℃$$

For Omega FPR300 Low Flow Meter:

Per calibration report, conducted at 15 and 2 GPM (the latter of which is will be used, as it is nearer the values experienced in the procedure), the Type B Uncertainty was 0.806 pulses per gallon at the 67% confidence interval. The minimum flow rate recommended in the report was 0.2 GPM, and the actual values were well above this.

$$U_{F(PPG)} = 0.806\ PPG$$

With 453.5 PPG, this equates to 0.0017 Gallon per minute error. This then equates to 1.07E-7 m^3/s.

$$U_{F(m^3/s)} = 1.07E-7\ m^3/s$$

$$q = \dot{m} c_p \Delta T$$

$$q = \dot{V} \rho c_p \Delta T$$

$$\delta q = \sqrt{\left(\frac{\partial q}{\partial \dot{V}} \delta \dot{V}\right)^2 + \left(\frac{\partial q}{\partial T} \delta T\right)^2}$$

Where

$$\dot{V} = 9.53E-5 \frac{m^3}{s}$$

$$\rho = 996 \frac{kg}{m^3}$$

$$c_p = 4191 \frac{J}{kgK}$$

The largest temperature differential occurs at the beginning of the run when the chilled water is at the set point and the tank temperature is still at approximately ambient. Since this differential is the result of subtracting one T-Type readout from another, the uncertainty from temperature is simply the sum of two T-Type uncertainties. The actual uncertainty may be lower considering there are three separate thermocouples on the rake, but since the thermocouples are at differing depths, this is a more conservative estimate of the error; the electric bubbler helps to mitigate stratification (a depth dependent variation of temperature due to the temperature dependence of water density) but

$$\Delta T = 13K$$

$$\delta q = \sqrt{(5.42E7 \times 1.07E-7)^2 + (397.805 \times 2(0.291))^2}$$

$$\delta q = 231.595\ J/s$$

With an instantaneous q-value of 5171.46 J/s,

$$\frac{\delta q}{q} * 100 = Percent\ Uncertainty$$

$$\frac{231.595}{5171.46} * 100 = 4.478\%\ Uncertainty$$

For Hanging Scale:

Uncertainty is stated as

$$U_{W(ozs)} = 2\ oz$$

In SI units this equates to

$$U_{W(kg)} = 0.05669\ kg$$

Where

$$Q = mL$$

$$\delta Q = \sqrt{\left(\frac{\partial Q}{\partial m}\delta m\right)^2}$$

For Water,

$$L = 334{,}000\ \frac{J}{kg}$$

$$\delta Q = \sqrt{(L\delta m)^2}$$

$$\delta Q = \sqrt{\left(334{,}000\ \frac{J}{kg}0.05669\ kg\right)^2}$$

$$\delta Q = 18{,}934.5\ J$$

At Linkage, ice has 2.5 MJ of energy stored, so

$$\frac{\delta Q}{Q} * 100 = Percent\ Uncertainty$$

$$\frac{18934.5J}{2.5E6} * 100 = 0.76\%\ Uncertainty$$

For PCM,

$$L = 178{,}000\ \frac{J}{kg}$$

$$\delta Q = \sqrt{(L\delta m)^2}$$

$$\delta Q = \sqrt{\left(178{,}000\ \frac{J}{kg} 0.05669\ kg\right)^2}$$

$$\delta Q = 10{,}090.8\ J$$

At 4.5 hours, PCM has 0.9 MJ of energy stored, so

$$\frac{\delta Q}{Q} * 100 = Percent\ Uncertainty$$

$$\frac{10{,}090.8\ J}{0.9E6} * 100 = 1.12\%\ Uncertainty$$

For Caliper:

Uncertainty is stated as

$$U_r = 0.1mm = 0.0001m$$

Once again,

$$Q = mL$$

Since the frozen layer builds as an annulus around the tube, the mass of the frozen material may be derived using the volume and density of the material as follows.

$$m = \rho[(\pi {r_{ice}}^2 L_{pipe}) - (\pi {r_o}^2 L_{pipe})]$$

$$m = \rho\pi L_{pipe}({r_{ice}}^2 - {r_o}^2)$$

Therefore

$$Q = \rho\pi L_{pipe}({r_{ice}}^2 - {r_o}^2)L$$

$$\delta Q = \sqrt{\left(\frac{\partial Q}{\partial r_{ice}}\delta r_{ice}\right)^2}$$

$$\delta Q = \sqrt{\left(2\rho\pi L_{pipe} L r_{ice} * \delta r_{ice}\right)^2}$$

For Water,

$$L = 334{,}000\ \frac{J}{kg}$$

$$\rho = 917 \frac{kg}{m^3}$$

$$L_{pipe} = 5.58m$$

At linkage, radius of the ice is

$$r_{ice} = 0.014m$$

$$\delta Q = \sqrt{(1.503E8 * 0.0001m)^2}$$

$$\delta Q = 15033.4J$$

At Linkage, ice has 2.5 MJ of energy stored, so

$$\frac{\delta Q}{Q} * 100 = Percent\ Uncertainty$$

$$\frac{15033.4J}{2.5E6} * 100 = 0.60\%\ Uncertainty$$

For PCM,

$$L = 178{,}000\ \frac{J}{kg}$$

$$\rho = 950 \frac{kg}{m^3}$$

$$L_{pipe} = 5.58m$$

At linkage, radius of the frozen PCM is

$$r_{ice} = 0.014m$$

$$\delta Q = \sqrt{(8.30E7 * 0.0001m)^2}$$

$$\delta Q = 8300.15J$$

At Linkage, PCM has 0.9 MJ of energy stored, so

$$\frac{\delta Q}{Q} * 100 = Percent\ Uncertainty$$

$$\frac{8300.15J}{0.9E6} * 100 = 0.92\%\ Uncertainty$$

Appendix D: PureTemp 8 Data Sheet

PureTemp®

PureTemp® Thermal Energy Storage Materials

PureTemp thermal energy storage materials offer new levels of performance in storing or releasing large quantities of thermal energy at any given temperature. Our proprietary formulations and patented manufacturing processes yield superior quality biobased phase change materials at cost effective prices.

Some key properties:

- Thermal energy storage capacities which average 200 J/g
- Over 200 unique, engineered phase change transition temperatures between -40 °C and 151 °C
- Consistent, repeatable performance over thousands of thermal (melt/solidify) cycles
- 100% renewable and readily biodegradable – produced from agricultural sources, not petroleum

PureTemp 8 Technical Information

PureTemp 8 is a USDA Certified Biobased product

Appearance	Clear liquid, waxy solid
Melting point	8 °C
Heat storage capacity	178 J/g
Thermal conductivity (liquid)	0.14 W/m°C
Thermal conductivity (solid)	0.22 W/m°C
Density (liquid)	0.86 g/ml
Density (solid)	0.95 g/ml
Specific heat (liquid)	2.15 J/g°C
Specific heat (solid)	1.85 J/g°C

Typical physical properties are listed in the table above.

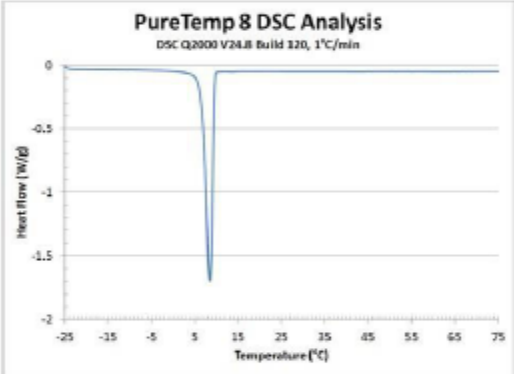

Thermal Cycle Stability

A thermal cycle stability study was performed on PureTemp 8 in which samples underwent a series of freeze and thaw cycles. The two year study completed 10,000 thermal cycles, with performance analyses performed on the samples at various time points. The study for PureTemp 8 found that:

- The average latent heat for PureTemp 8, over the course of 10,000 cycles, passes the product specification.
- PureTemp 8 maintained a peak melting point of 8.5 ± 0.1 °C.

PureTemp 8 is stable through 10,000 thermal cycles, which is approximately 27.4 years of continuous daily usage.

Entropy Solutions, LLC.
4232 Park Glen Road, Minneapolis, MN 55416
Tel: +1-952-941-0306
Inquiry: www.puretemp.com/contact
Website: www.puretemp.com

USDA CERTIFIED BIOBASED PRODUCT
PRODUCT 100%

Appendix E: Matlab Code

Sensible Water Cooldown:

```
t= 0:20000; % time array in seconds
thours= t/3600; % time array in hours
desiredtemp= 5; % Temperature we want the tank to get to
Waterdensity= 999.3664;
Viscwater= 1.21*10^-3; %Dynamic viscosity of water.
Cpwater=4188.996; %Specific Heat of water
kwater= 0.585004; %Thermal conductivity of water
kpipe= 0.33; %thermal conductivity of the Pipe
kbucket = 0.45; %Thermal Conductivity of the bucket
kins = 0.00635; %Thermal Conductivity of the insulation
IDpipe= 0.0127; %inner diameter of pipe in m
IRpipe= IDpipe/2;
ODpipe= 0.0166;%outer diameter of pipe in meters
ORpipe= ODpipe/2;
PipeFeet= 17.31 ; % pipe length in feet
Lengthofpipe= 0.3048* PipeFeet; %pipe length converted to meters


bucketIR= 0.14605;
bucketwallthick= 0.0025; %meters
bucketinsthick= 0.01905; %insulation thickness meters
bucketheight= 0.254;

bucketID= 2*bucketIR;
bucketOD= 2*bucketIR+2*bucketwallthick;
bucketOR= bucketOD/2;
bucketinsOD= 2*bucketIR+2*bucketwallthick+2*bucketinsthick;
bucketinsOR= bucketinsOD/2;

bucketvolume=pi * (bucketIR)^2 * bucketheight;

diamhelix= bucketID-0.05;
massofwater= Waterdensity*bucketvolume;
gpm= 2.19;
volumeflowrate= (6.309*(10^-5)*gpm); %volume flow rate in cubic meters per second
massflowrate= volumeflowrate * Waterdensity;
Re= (4 * massflowrate)/(pi*(IDpipe)*(Viscwater)); %Reynolds number
Pr= (Viscwater*Cpwater)/kwater; %Prantl Number
De= Re*sqrt(IDpipe/diamhelix);
StraightNusselt=0.023*(Re)^(4/5)* (Pr)^(0.4);
hi= 0.023*(Re)^(4/5)* (Pr)^(0.4)*(kwater/IDpipe); %Calculation of internal heat
transfer coefficient
ho= 1000; %outer wall film coefficient
Tinitial= 19.0; %initial tank temperature
Troom= 16.9; % Room temperature
Tcoolin= 4.5; %temperature of cooling water in Celsius 4.5
hroom= 8; %Heat transfer coefficient of the bucket to the room

UAbucket=
1/((1/(ho*pi*2*bucketIR*bucketheight))+(log(bucketOR/bucketIR)/(2*pi*bucketheight*kbuc
ket))+(log(bucketinsOR/bucketOR)/(2*pi*bucketheight*kins))+(1/(hroom*pi*2*bucketOR*buc
ketheight)));

CriticalREnorm= 2300;
CriticalREhelix= CriticalREnorm*(1+12*(IDpipe/diamhelix)^0.5);
aNU=1+(957*(diamhelix/IDpipe)/(Re^2*Pr));
bNU=1+0.477/Pr;
dynviscwater7C= 0.00143;
```

```
dynviscwater4C= 0.00157;

NUhelix= ((3.66+(4.343/aNU))^3
+1.158*((Re*(IDpipe/diamhelix)^(1/2))/bNU)^(3/2))^(1/3)*(dynviscwater4C/dynviscwater7C
)^0.14;
hihelix= NUhelix*(kwater/IDpipe);
UAhelix=1/((1/(hihelix*pi*2*IRpipe*Lengthofpipe))+(log(ORpipe/IRpipe)/(2*pi*Lengthofpi
pe*kpipe))+(1/(ho*pi*2*ORpipe*Lengthofpipe)));
tconsthelix= (Waterdensity*bucketvolume*Cpwater)/(massflowrate*Cpwater*(1-exp((-
UAhelix)/(massflowrate*Cpwater))));
ahel= (massflowrate*Cpwater-massflowrate*Cpwater*exp((-
UAhelix)/(massflowrate*Cpwater))+UAbucket)/(Waterdensity*bucketvolume*Cpwater);
boahelix= (Tcoolin*(massflowrate*Cpwater-massflowrate*Cpwater*exp((-
UAhelix)/(massflowrate*Cpwater)))+UAbucket*Troom)/(massflowrate*Cpwater-
massflowrate*Cpwater*exp((-UAhelix)/(massflowrate*Cpwater))+UAbucket);
Ttankhelix= (Tinitial-boahelix)*exp(-ahel*t)+boahelix;
Tcoolout= Ttankhelix+(Tcoolin-Ttankhelix)*(exp((-UAhelix)/(massflowrate*Cpwater)));
qdouble2= massflowrate*Cpwater*-(Tcoolin-Tcoolout); %finds heat transfer rate from
difference between theoretical water in and out temps
Theorytempdiff= Tcoolin -Tcoolout;


Q=cumtrapz(qdouble2); %Find energy stored by taking the integral of qdouble2

DAQrawdata= load('PDAQ.MAT');
whos -file PDAQ.MAT
%DAQrawdata (prints all raw data)
DAQbttm= DAQrawdata.A(:,[1].');
DAQmid= DAQrawdata.A(:,[2]);
DAQtop= DAQrawdata.A(:,[3]);
DAQcws= DAQrawdata.A(:,[4]);
DAQcwr= DAQrawdata.A(:,[5]);
DAQamb= DAQrawdata.A(:,[6]);
tdaq= 0:4918;
tdaqhours= tdaq/(3600/3.68916);


SteadyTdiff= mean(DAQcwr(4000:4919))-mean(DAQcws(4000:4919));% for use when looking at
difference in inlet and outlet temps
DeltaT=DAQcws-(DAQcwr-SteadyTdiff); %difference between cold water send and return
temp  (the flllowing removes steady state heat gain) DAQcws - (DAQcwr-SteadyTdiff)

qdoubactual= massflowrate*Cpwater*-DeltaT;%uses heat gain from water sent

[Tempfit,gof]= fit(tdaqhours.',DAQmid,'exp2');%create exponential fit curve for middle
temp profile
diffTempfit= differentiate(Tempfit,tdaqhours);

[qdoubfit,gof]= fit(tdaqhours.',qdoubactual,'exp2');
Qcurvefit= integrate(qdoubfit,tdaqhours,0);

tiledlayout(2,3)
nexttile


plot(thours,Ttankhelix,'g')
hold on
yline(desiredtemp);
plot(Tempfit,tdaqhours,DAQmid, 'b')
hold on
plot(tdaqhours,DAQbttm, 'r')
hold on
plot(tdaqhours,DAQmid, 'b')
```

```
hold on
plot(tdaqhours,DAQtop, 'k')
hold on

legend('Theoretical Tank Temperature','Desired Tank Temperature','Fitted Actual Tank
Temperature', 'Bottom Thermocouple Raw Data','Middle Thermocouple Raw Data','Top
Thermocouple Raw Data')
title('Tank Temperature vs. Time')
xlabel('Time (hrs)')
ylabel('Temperature (°C)')

nexttile

plot(tdaqhours,DAQcws, 'c')
hold on
plot(tdaqhours,DAQcwr, 'm')
hold on
plot(tdaqhours,DAQamb, 'y')
legend({'Chilled Fluid Send Temperature','Chilled Fluid Return Temperature', 'Ambient
Temperature'},'Location','east')
title('Various Temperatures vs. Time')
xlabel('Time (hrs)')
ylabel('Temperature (°C)')

nexttile

plot(qdoubfit,tdaqhours,qdoubactual, 'b')
hold on
plot(thours,qdouble2,'g');
hold on
legend('Raw Heat Transfer Data','Curve Fit for Heat Transfer', 'Theoretical Heat
Transfer')
xlabel('Time (hrs)')
ylabel('q(W)')
title('Heat Transfer (W) vs. Time')
xlim([0 6])
ylim([-50 700])


hold on

nexttile
plot(thours,Q,'g')
title('Energy Stored (J) vs. Time')
xlabel('Time (hrs)')
ylabel('Q(J)')
hold on
plot(tdaqhours,3600*Qcurvefit,'b');
hold on
legend({'Theoretical Stored Energy','Actual Stored Energy'},'Location','southeast')



%Dittus Boelter Nusselt
DittusReRange= 10000:15000;
DittusNusselt=0.023*(DittusReRange).^(4/5)* (Pr)^(0.4);

HelixRange= 0:15000;
ChartNUhelix= ((3.66+(4.343./(1+(957.*(diamhelix/IDpipe)./(HelixRange.^2*Pr))))).^3
+1.158.*((HelixRange.*(IDpipe/diamhelix).^(1/2))./bNU).^(3/2)).^(1/3)*(dynviscwater4C.
/dynviscwater7C).^0.14;

LaminarRange= 0:2300;
```

```
LaminarNusselt= zeros(2301,1);
LaminarNusselt(:)=3.66;

nexttile
plot(DittusReRange,DittusNusselt,'r')
hold on
plot(HelixRange,ChartNUhelix,'b')
hold on
plot(LaminarRange,LaminarNusselt,'g')
title('Nusselt Number vs. Reynolds Number for Straight and Helical Coils')
xlabel('Reynolds Number)')
ylabel('Nusselt Number)')

legend({'Dittus Boelter Straight Tube','Manlapaz-Churchill Helical Coiled
Tube','Laminar Pipe Flow'},'Location','west')

hold off
```

Latent Ice Building :

```
t= 0:20000; % time array in seconds
thours= t/3600; % time array in hours.
desiredtemp= 0; % Temperature we want the tank to get to
Waterdensity= 1063; %of 70% water/Ethelene glycol mix (by volume)
Viscwater= 0.00489; %Dynamic viscosity of 70% water/Ethelene glycol mix (by volume)
Cpwater=3569; %Specific Heat of 70% water/Ethelene glycol mix (by volume)@ -10*C
kwater= 0.466; %Thermal conductivity of  70% water/ 30% Ethelene glycol mix (by
volume)@ -10*C
kpipe= 0.33; %thermal conductivity of the Pipe
kbucket = 0.45; %Thermal Conductivity of the bucket
kins = 0.00635; %Thermal Conductivity of the insulation
IDpipe= 0.0127; %inner diameter of pipe in m
IRpipe= IDpipe/2;
ODpipe= 0.0166;%outer diameter of pipe in meters
ORpipe= ODpipe/2;
PipeFeet= 17.31 ; % pipe length in feet
Lengthofpipe= 0.3048* PipeFeet; %pipe length converted to meters


bucketIR= 0.14605;
bucketwallthick= 0.0025; %meters
bucketinsthick= 0.01905; %insulation thickness meters
bucketheight= 0.254;

bucketID= 2*bucketIR;
bucketOD= 2*bucketIR+2*bucketwallthick;
bucketOR= bucketOD/2;
bucketinsOD= 2*bucketIR+2*bucketwallthick+2*bucketinsthick;
bucketinsOR= bucketinsOD/2;

bucketvolume=pi * (bucketIR)^2 * bucketheight;

diamhelix= bucketID-0.05;
massofwater= Waterdensity*bucketvolume;
gpm= 0.91; %volume flow rate in gallons
volumeflowrate= (6.309*(10^-5)*gpm); %volume flow rate in cubic meters per second
massflowrate= volumeflowrate * Waterdensity;
Re= (4 * massflowrate)/(pi*(IDpipe)*(Viscwater)); %Reynolds number
Pr= (Viscwater*Cpwater)/kwater; %Prantl Number
De= Re*sqrt(IDpipe/diamhelix);
hi= 0.023*(Re)^(4/5)* (Pr)^(0.4)*(kwater/IDpipe); %Calculation of internal heat
transfer coefficient
ho= 1000; %outer wall film coefficient
UA=1/((1/(hi*pi*IDpipe*Lengthofpipe))+(log(ODpipe/IDpipe)/(2*pi*Lengthofpipe*kpipe))+(
1/(ho*pi*ODpipe*Lengthofpipe))); %overall heat transfer coefficient
tconst= (Waterdensity*bucketvolume*Cpwater)/(massflowrate*Cpwater*(1-exp((-
UA)/(massflowrate*Cpwater)))); %time constant
Tinitial= 16.0; %initial tank temperature
Troom= 16.9; % Room temperature
Tcoolin= -6; %temperature of cooling water in Celsius -6
hroom= 5; %Heat transfer coefficient of the bucket to the room

UAbucket=
1/((1/(ho*pi*2*bucketIR*bucketheight))+(log(bucketOR/bucketIR)/(2*pi*bucketheight*kbuc
ket))+(log(bucketinsOR/bucketOR)/(2*pi*bucketheight*kins))+(1/(hroom*pi*2*bucketOR*buc
ketheight)));

CriticalREnorm= 2300;
CriricalREhelix= CriticalREnorm*(1+12*(IDpipe/diamhelix)^0.5);
aNU=1+(957*(diamhelix/IDpipe)/(Re^2*Pr));
bNU=1+0.477/Pr;
```

```
dynviscwater7C= 0.00489;
dynviscwater4C= 0.00489;

NUhelix= ((3.66+(4.343/aNU))^3
+1.158*((Re*(IDpipe/diamhelix)^(1/2))/bNU)^(3/2))^(1/3)*(dynviscwater4C/dynviscwater7C
)^0.14;
hihelix= NUhelix*(kwater/IDpipe);


Tf= 0; %freezing point of (water)
L= 334000; %latent heat of freezing water (J/kg*K)
Cpice= 2093; %J/kgK
St= (Cpice*(Tf- Tcoolin))/L;

kice= 2.22; %W/mK
densice= 919; %kg/m^3

rstep= 0:25000;
ORice= ORpipe+0.011;
rice= (ORpipe)+((ORice)*(rstep/25000)); %ice radius


Tice= ((Tf-
Tcoolin)/((kice/(ho*(ODpipe)))+exp((ORice)/(ODpipe))))*(exp(rice/(ODpipe)))+Tcoolin;

Uvalue=((pi*ODpipe*Lengthofpipe)/(pi*IDpipe*Lengthofpipe*hihelix)+((pi*ODpipe*Lengthof
pipe)*log(ORpipe/IRpipe))/(2*pi*kpipe*Lengthofpipe))^-1;
Uvaluein=((pi*IDpipe*Lengthofpipe)/(pi*IDpipe*Lengthofpipe*hihelix)+((pi*IDpipe*Length
ofpipe)*log(ORpipe/IRpipe))/(2*pi*kpipe*Lengthofpipe))^-1;

timeice=((densice.*L)./(kice.*(Tf-Tcoolin))).*(0.5.*(rice.^2).*log(rice./(ORpipe))-
(0.25.*(rice.^2-ORpipe.^2)).*(1-((2.*kice)./(Uvalue.*(ORpipe)))));


timeicehours= timeice/3600;

Latentheat= densice*pi*Lengthofpipe*((rice.^2)-(ORpipe^2))*L;
tiledlayout(2,2)
nexttile
plot(timeicehours+.95,rice,'g'); %Latent cooldown begins at 0.95 hrs
hold on

massofice=[0.34,1.31,1.44,2.32,2.58,2.78,3.5,4.04];
%0,0.34,1.31,1.44,2.32,2.58,2.78,3.5,4.04
timeofweight=[679,881,1091,1304,1508,1712,1916,2124];%[481,679,881,1091,1304,1508,1712
,1916,2124
timeofweighthours= timeofweight/(618.666);
Iceradius= sqrt((massofice/(densice*pi*Lengthofpipe))+(ORpipe)^2);
plot(timeofweighthours,Iceradius,'o');
hold on

timeofweightcaliper=[679,881,1091,1304,1508,1712];%[481,679,881,1091,1304,1508,1712]
timeofweightcaliperhours= timeofweightcaliper/(618.666);
Iceradiuscaliper=[0.0173/2,0.0211/2,0.0241/2,0.0269/2,0.0290/2,0.0309/2];%[0.0164/2,0.
0173/2,0.0211/2,0.0241/2,0.0269/2,0.0290/2,0.0309/2]
plot(timeofweightcaliperhours,Iceradiuscaliper,'s','MarkerEdge',[0.3010,0.7450,0.9330]
);
hold on


%create log fits to raw data points
x = timeofweighthours';
y = Iceradius';
```

```
x2= timeofweightcaliperhours';
y2= Iceradiuscaliper';
myfittype = fittype('a + b*log(x)',...
    'dependent',{'y'},'independent',{'x'},...
    'coefficients',{'a','b'})
logfitweight = fit(x,y,myfittype)
logfitcaliper= fit(x2,y2,myfittype)
plot(logfitweight);
plot(logfitcaliper, 'b');
logfitweightradii= feval(logfitweight, timeicehours(7001:end)); %turn curve into an
array by exavluating at points
logfitcaliperradii= feval(logfitcaliper, timeicehours(7001:end));

xlabel('Time (hrs)')
ylabel('Ice Radius (m)')
title('Ice Radius (m) vs. Time  ')
xlim([0 3.5])
ylim([0.0075, 0.02])
legend({'Theoretical Ice Radius','Actual Ice Radius by Weight','Actual ice Radius by
Caliper Measurement', 'Weight Radius Curve Fit', 'Caliper Radius curve
fit'},'Location','northwest')


nexttile

DAQRawData= load('ICE_Building_2-22-21.MAT');
whos -file ICE_Building_2-22-21.MAT
%DAQrawdata (prints all raw data)
DAQbttm2= DAQRawData.A(:,[1].');
DAQmid2= DAQRawData.A(:,[2]);
DAQtop2= DAQRawData.A(:,[3]);
DAQcws2= DAQRawData.A(:,[4]);
DAQcwr2= DAQRawData.A(:,[5]);
DAQamb2= DAQRawData.A(:,[6]);
DAQsurf1two= DAQRawData.A(:,[7]);
DAQsurf2two= DAQRawData.A(:,[8]);
DAQsurf3two= DAQRawData.A(:,[9]);

tdaq2= 0:2141;
tdaqhours2= tdaq2/(618.666);



SteadyTdiff=mean(DAQcwr2(1800:2142))-mean(DAQcws2(1800:2142));%for use when looking at
difference in inlet and outlet temps
DeltaT=DAQcws2-(DAQcwr2-SteadyTdiff); %difference between cold water send and return
temp  (the flllowing removes steady state heat gain) DAQcws - (DAQcwr-SteadyTdiff)

qdoubinout= -massflowrate*Cpwater*DeltaT;%uses heat gain from water sent


[qdoubfit,gof]= fit(tdaqhours2.',qdoubinout,'exp2');

plot(tdaqhours2,DAQamb2)
hold on

plot(tdaqhours2,DAQbttm2)
hold on
plot(tdaqhours2,DAQmid2)
hold on
plot(tdaqhours2,DAQtop2,'k')
hold on
```

```
plot(tdaqhours2,DAQsurf1two)
hold on
plot(tdaqhours2,DAQsurf2two)
hold on
plot(tdaqhours2,DAQsurf3two)
hold on
plot(tdaqhours2,DAQcwr2)
hold on
plot(tdaqhours2,DAQcws2)
hold on
legend('Ambient Temperature','Bottom Thermocouple Raw Data','Middle Thermocouple Raw
Data','Top Thermocouple Raw Data','Coil Surface Temperature (Inlet)','Coil Surface
Temperature (Middle)', 'Coil Surface Temperature (Outlet)','Coolant Return
Temperature','Coolant Send Temperature')
title('Tank Temperature vs. Time')
xlabel('Time (hrs)')
ylabel('Temperature (˚C)')

nexttile

sensibleportion= bucketvolume*Waterdensity*Cpwater*15;
plot(timeicehours+0.95,Latentheat+sensibleportion,'g');
hold on
Latentheatfromweight= densice*pi*Lengthofpipe*((logfitweightradii.^2)-(ORpipe^2))*L;
Latentheatfromcaliper= densice*pi*Lengthofpipe*((logfitcaliperradii.^2)-(ORpipe^2))*L;
plot(timeicehours(7001:end),Latentheatfromweight+sensibleportion,'r');
plot(timeicehours(7001:end),Latentheatfromcaliper+sensibleportion,'b');
xlim([0 3.5])
title('Sensible + Latent Energy Stored (J) vs. Time')
xlabel('Time (hrs)')
ylabel('Q(J)')
hold on
legend({'Theoretical Stored Energy','Actual Stored Energy (weight)','Actual Stored
Energy (caliper)'},'Location','northwest')



nexttile

timeice2= timeice;
timeice2 (25001)= [];
timeicehours2=timeicehours(7001:end);
timeicehours2(18001)= [];
dQ= Latentheat(7002:end) - Latentheat(7001:end-1);
dt = timeice(7002:end) - timeice(7001:end-1);
qdoubletheory= dQ./dt;
LHFW2=Latentheatfromweight.';
LHFC2=Latentheatfromcaliper.';
dQweight= LHFC2(2:end) - LHFC2(1:end-1);
qdoubleactual= dQweight./dt;


plot(timeicehours2,qdoubletheory,'g');
hold on

plot(timeicehours2,qdoubleactual,'c');
hold on
xlim([0 3.5])
ylim([0 500])
title('Heat Transfer Rate (W) vs. Time')
xlabel('Time (hrs)')
ylabel('q (W)')
```

```
legend('Theoretical Heat Transfer','Actual Heat Transfer (from Weight)')
hold off
```

Latent PCM Freezing

```
t= 0:20000; % time array in seconds
thours= t/3600; % time array in hours
desiredtemp= 5; % Temperature we want the tank to get to
Waterdensity= 999.3664;
Viscwater= 1.21*10^-3; %Dynamic viscosity of water.
Cpwater=4188.996; %Specific Heat of water
kwater= 0.585004; %Thermal conductivity of water
kpipe= 0.33; %thermal conductivity of the Pipe
kbucket = 0.45; %Thermal Conductivity of the bucket
kins = 0.00635; %Thermal Conductivity of the insulation
IDpipe= 0.0127; %inner diameter of pipe in m
IRpipe= IDpipe/2;
ODpipe= 0.0166;%outer diameter of pipe in meters
ORpipe= ODpipe/2;
PipeFeet= 17.31 ; % pipe length in feet
Lengthofpipe= 0.3048* PipeFeet; %pipe length converted to meters


bucketIR= 0.14605;
bucketwallthick= 0.0025; %meters
bucketinsthick= 0.01905; %insulation thickness meters
bucketheight= 0.254;

bucketID= 2*bucketIR;
bucketOD= 2*bucketIR+2*bucketwallthick;
bucketOR= bucketOD/2;
bucketinsOD= 2*bucketIR+2*bucketwallthick+2*bucketinsthick;
bucketinsOR= bucketinsOD/2;

bucketvolume=pi * (bucketIR)^2 * bucketheight;


diamhelix= bucketID-0.05;
massofwater= Waterdensity*bucketvolume;
gpm= 1.50; %volume flow rate in gallons
volumeflowrate= (6.309*(10^-5)*gpm); %volume flow rate in cubic meters per second
massflowrate= volumeflowrate * Waterdensity;
Re= (4 * massflowrate)/(pi*(IDpipe)*(Viscwater)); %Reynolds number
Pr= (Viscwater*Cpwater)/kwater; %Prandtl Number
De= Re*sqrt(IDpipe/diamhelix);
ratio=sqrt(IDpipe/diamhelix);
hi= 0.023*(Re)^(4/5)* (Pr)^(0.4)*(kwater/IDpipe); %Calculation of internal heat
transfer coefficient
ho= 1000; %outer wall film coefficient
UA=1/((1/(hi*pi*IDpipe*Lengthofpipe))+(log(ODpipe/IDpipe)/(2*pi*Lengthofpipe*kpipe))+(
1/(ho*pi*ODpipe*Lengthofpipe))); %overall heat transfer coefficient
tconst= (Waterdensity*bucketvolume*Cpwater)/(massflowrate*Cpwater*(1-exp((-
UA)/(massflowrate*Cpwater)))); %time constant
Tinitial= 22.0; %initial tank temperature
Troom= 22.0; % Room temperature
Tcoolin= 4.5; %temperature of cooling water in Celsius
hroom= 5; %Heat transfer coefficient of the bucket to the room

UAbucket=
1/((1/(ho*pi*2*bucketIR*bucketheight))+(log(bucketOR/bucketIR)/(2*pi*bucketheight*kbuc
ket))+(log(bucketinsOR/bucketOR)/(2*pi*bucketheight*kins))+(1/(hroom*pi*2*bucketOR*buc
ketheight)));

CriticalREnorm= 2300;
CriricalREhelix= CriticalREnorm*(1+12*(IDpipe/diamhelix)^0.5);
aNU=1+(957*(diamhelix/IDpipe)/(Re^2*Pr));
```

```
bNU=1+0.477/Pr;
dynviscwater7C= 0.00143;
dynviscwater4C= 0.00157;

NUhelix= ((3.66+(4.343/aNU))^3
+1.158*((Re*(IDpipe/diamhelix)^(1/2))/bNU)^(3/2))^(1/3)*(dynviscwater4C/dynviscwater7C
)^0.14;
hihelix= NUhelix*(kwater/IDpipe);


Tf= 7; %freezing point PCM
L= 178000; %latent heat of freezing PCM (J/kg*K)
CpLiquidPCM= 2150; %J/kgC from kelseylee (Schafer, 2016)
CpSolidPCM= 1850; %J/kgC from kelseylee (Schafer, 2016)
St= (CpSolidPCM*(Tf- Tcoolin))/L;

kice= 0.22; %W/mK  for phase change material
densice= 950; %kg/m^3

rstep= 0:25000;
ORice= ORpipe+0.011;
rice= (ORpipe)+((ORice)*(rstep/25000)); %ice radius


Tice= ((Tf-
Tcoolin)/((kice/(ho*(ODpipe)))+exp((ORice)/(ODpipe))))*(exp(rice/(ODpipe)))+Tcoolin;

Uvalue=((pi*ODpipe*Lengthofpipe)/(pi*IDpipe*Lengthofpipe*hihelix)+((pi*ODpipe*Lengthof
pipe)*log(ORpipe/IRpipe))/(2*pi*kpipe*Lengthofpipe))^-1;
Uvaluein=((pi*IDpipe*Lengthofpipe)/(pi*IDpipe*Lengthofpipe*hihelix)+((pi*IDpipe*Length
ofpipe)*log(ORpipe/IRpipe))/(2*pi*kpipe*Lengthofpipe))^-1;


timeice=((densice.*L)./(kice.*(Tf-Tcoolin))).*(0.5.*(rice.^2).*log(rice./(ORpipe))-
(0.25.*(rice.^2-ORpipe.^2)).*(1-((2.*kice)./(Uvalue.*(ORpipe)))));

timeicehours= timeice/3600;


Latentheat= densice*pi*Lengthofpipe*((rice.^2)-(ORpipe^2))*L;
tiledlayout(2,2)

nexttile
plot(timeicehours+0.75,rice,'g'); %Freezing achieved at 0.75 hrs
hold on
massofice=[0,0.45,0.61,0.96,1.16,1.4,1.62,1.71,1.75,2.33,2.72,2.6];
timeofweight=[549,761,966,1167,1377,1585,1792,1998,2202,2614,3028,3234];

timeofweighthours= timeofweight/(753.5); %(3600/3.68916)
Iceradius= sqrt((massofice/(densice*pi*Lengthofpipe))+(ORpipe)^2);
plot(timeofweighthours,Iceradius,'o');
hold on

timeofweightcaliper=[549,761,966,1167,1377,1585,1792,1998,2202,2614,3028,3234];
timeofweightcaliperhours= timeofweightcaliper/(753.5);%(3600/3.68916)
Iceradiuscaliper=[0.007966667,0.0093,0.010283333,0.0107,0.0112,0.011616667,0.012033333
,0.01265,0.01285,0.013583333,0.014533333,0.01425];
plot(timeofweightcaliperhours,Iceradiuscaliper,'s','MarkerEdge',[0.3010,0.7450,0.9330]
);
hold on


%create log fits to raw data points
```

```
x = timeofweighthours';
y = Iceradius';
x2= timeofweightcaliperhours';
y2= Iceradiuscaliper';
myfittype = fittype('a + b*log(x)',...
    'dependent',{'y'},'independent',{'x'},...
    'coefficients',{'a','b'})
logfitweight = fit(x,y,myfittype)
logfitcaliper= fit(x2,y2,myfittype)
plot(logfitweight);
plot(logfitcaliper, 'b');
logfitweightradii= feval(logfitweight, timeicehours(3001:end)); %turn curve into an
array by exavluating at points
logfitcaliperradii= feval(logfitcaliper, timeicehours(3001:end));

xlabel('Time (hrs)')
ylabel('PCM Radius (m)')
title('PCM Radius (m) vs. Time')
xlim([0 4.5])
ylim([0.0075, 0.02])
legend({'Theoretical PCM Radius','Actual PCM Radius by Weight','Actual PCM Radius by
Caliper Measurement', 'Weight Radius Curve Fit', 'Caliper Radius curve
fit'},'Location','northwest')


nexttile

DAQRawData= load('PCM_5-6-21.MAT');
whos -file PCM_5-6-21.MAT
%DAQrawdata (prints all raw data)
DAQbttm2= DAQRawData.A(:,[1].');
DAQmid2= DAQRawData.A(:,[2]);
DAQtop2= DAQRawData.A(:,[3]);
DAQcws2= DAQRawData.A(:,[4]);
DAQcwr2= DAQRawData.A(:,[5]);
DAQamb2= DAQRawData.A(:,[6]);
DAQsurf1two= DAQRawData.A(:,[7]);
DAQsurf2two= DAQRawData.A(:,[8]);
DAQsurf3two= DAQRawData.A(:,[9]);

tdaq2= 0:3284;
tdaqhours2= tdaq2/(753.5);



SteadyTdiff=mean(DAQcwr2(1800:2142))-mean(DAQcws2(1800:2142));%for use when looking at
difference in inlet and outlet temps
DeltaT=DAQcws2-(DAQcwr2-SteadyTdiff); %difference between cold water send and return
temp  (the flllowing removes steady state heat gain) DAQcws - (DAQcwr-SteadyTdiff)

qdoubinout= -massflowrate*Cpwater*DeltaT;%uses heat gain from water sent


[qdoubfit,gof]= fit(tdaqhours2.',qdoubinout,'exp2');


plot(tdaqhours2,DAQamb2)
hold on

plot(tdaqhours2,DAQbttm2)
hold on
plot(tdaqhours2,DAQmid2,'k')
hold on
```

```
plot(tdaqhours2,DAQtop2)
hold on
plot(tdaqhours2,DAQsurf1two)
hold on
plot(tdaqhours2,DAQsurf2two)
hold on
plot(tdaqhours2,DAQsurf3two)
hold on
plot(tdaqhours2,DAQcwr2)
hold on
plot(tdaqhours2,DAQcws2)
hold on


legend('Ambient Temperature','Bottom Thermocouple Raw Data','Middle Thermocouple Raw
Data','Top Thermocouple Raw Data','Coil Surface Temperature (Inlet)','Coil Surface
Temperature (Middle)', 'Coil Surface Temperature (Outlet)','Coolant Return
Temperature','Coolant Send Temperature')
title('Tank Temperature vs. Time')
xlabel('Time (hrs)')
ylabel('Temperature (°C)')

nexttile


cppcmliquid=2150; %J/kg*C
DensityLiquidPCM= 860; %kg/m^3


sensibleportion= bucketvolume*DensityLiquidPCM*cppcmliquid*13;

plot(timeicehours+0.75,Latentheat+sensibleportion,'g');
hold on
Latentheatfromweight= densice*pi*Lengthofpipe*((logfitweightradii.^2)-(ORpipe^2))*L;
Latentheatfromcaliper= densice*pi*Lengthofpipe*((logfitcaliperradii.^2)-(ORpipe^2))*L;
plot(timeicehours(3001:end),Latentheatfromweight+sensibleportion,'r');
plot(timeicehours(3001:end),Latentheatfromcaliper+sensibleportion,'b');
xlim([0 4.5])
title('Sensible + Latent Energy Stored (J) vs. Time')
xlabel('Time (hrs)')
ylabel('Q(J)')
hold on
legend({'Theoretical Stored Energy','Actual Stored Energy from Weight','Actual Stored
Energy from Caliper'},'Location','northwest')

nexttile
timeice2= timeice;
timeice2 (25001)= [];
timeicehours2=timeicehours(3001:end);
timeicehours2(21001)= [];
dQ= Latentheat(3002:end) - Latentheat(3001:end-1);
dt = timeice(3002:end) - timeice(3001:end-1);
qdoubletheory= dQ./dt;
LHFW2=Latentheatfromweight.';
LHFC2=Latentheatfromcaliper.';
dQweight= LHFC2(2:end) - LHFC2(1:end-1);
qdoubleactual= dQweight./dt;



plot(timeicehours2,qdoubletheory,'g');
hold on
```

```
plot(timeicehours2,qdoubleactual,'c');
hold on
xlim([0 4.5])
ylim([0 550])

title('Heat Transfer Rate (W) vs. Time')
xlabel('Time (hrs)')
ylabel('q (W)')

legend('Theoretical Heat Transfer','Actual Heat Transfer (from Weight)')

hold off
```

Appendix F: Similar Temperature Extrapolation

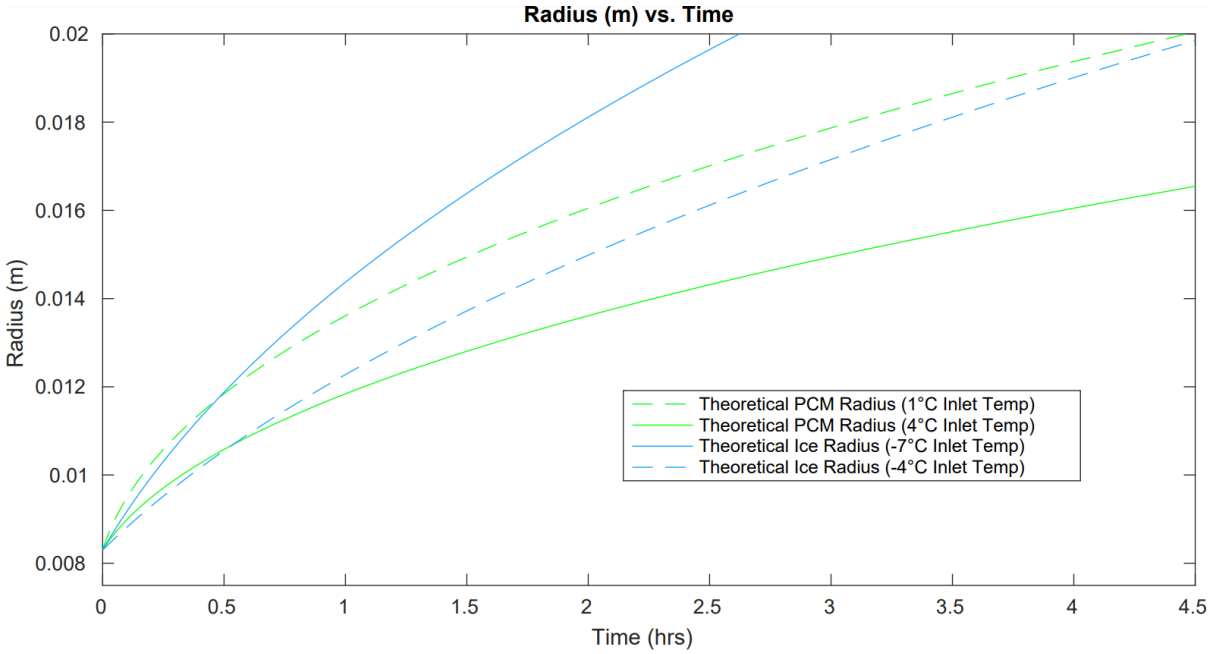

Figure 20. Analytical Model Applied to Similar Temperature Differentials for Ice and PCM

As mentioned previously, the driving temperature differential for the Ice and PCM experimental runs were different; Ice was seven degrees below the nominal freezing point of water, and PCM was four degrees below its nominal freezing point (to accurately represent the common HVAC evaporator temperature that would be used to cool it in reality). Since the analytical model fit both of these cases well, despite having entirely different storage and coolant media properties, the model may be used to extrapolate the runs. Here, theory is shown for each media cooled with a temperature four and seven degrees below its freezing point. At small time, both PCM cases outperform the ice building, due to the higher heat transfer coefficient achieved with pure water as coolant. Before the half hour mark after initial freezing, both water cases surpass their counterpart, due to the better thermal conductivity of ice. It should be noted that with different coolant temperatures, the sensible cooldown of these media would occur at different times, but for the sake of comparison in this plot, freezing for all four cases begins at zero-time.